bioRxiv preprint doi: https://doi.org/10.1101/777649; this version posted September 23, 2019. The copyright holder for this preprint (which was not certified by peer review) is the author/funder, who has granted bioRxiv a license to display the preprint in perpetuity. It is made available under aCC-BY-NC-ND 4.0 International license.

The lipid kinase PI3Kα is required for aggregation and survival of intraperitoneal cancer cells.

96 characters – 100 max

Authors

Thole A [1,2], Thibault B [1,2], Basset C [1,2,3], Guillermet-Guibert J [1,2]*.

1 : INSERM – UMR 1037 – Equipe 17, Toulouse
2 : LABEX TouCAN, Toulouse
3 : Service d'Anatomo-Pathologie Institut Universitaire du Cancer de Toulouse – Oncopole (IUCT-O), Toulouse

***corresponding author:** Julie Guillermet-Guibert
CRCT UMR1037 INSERM-Université Toulouse 3 - ERL5294 CNRS; 2 avenue Hubert Curien; Oncopole de Toulouse; CS 53717; 31037 TOULOUSE CEDEX 1 - FRANCE
Tel : +33-(0) 5 82 74 16 52
e-mail: julie.guillermet@inserm.fr
http://www.crct-inserm.fr/17-j-guillermet-guibert-sigdyn-group-pi3k-isoforms-signalling-cancerogenesis-559.html
http://eupancreas.com/julie-guillermet-guibert
http://pi3k-phdproject.eu/partner/julie-guillermet-guibert/

Running Title 38 – max 40

PI3Kα controls tumour cell aggregation

SUMMARY (174 WORDS) - MAX 175 WORDS

Peritoneal carcinomatosis in ovarian cancer is often associated with ascites. In malignant ascites, tumour isolated cells and cell aggregates were present with a variability in size and numbers. Addition of mesenchymal stem cells, as a model of tumoural stroma, favoured aggregation of tumour cells. Because of the emerging concept that tri-dimensional cell culture could lead to increased resistance to conventional therapies, we investigated the importance of PI3Kα-driven pro-tumourigenic and pro-chemoresistance signal in the formation of 3D model of ovarian cancer ascites. We demonstrated, through the use of selective pharmacological inhibitors of the PI3Kα isoform, the key role of this enzyme in the formation and maintenance of multicellular aggregates from ovarian origin. This role did not depend solely on a pro-survival activity of PI3Kα, but could be linked to changes in cell/cell adhesion. Finally, PI3Kα-selective inhibitors were also equally efficient in the presence of cisplatin. We hence identified a signaling pathway of interest for the

bioRxiv preprint doi: https://doi.org/10.1101/777649; this version posted September 23, 2019. The copyright holder for this preprint (which was not certified by peer review) is the author/funder, who has granted bioRxiv a license to display the preprint in perpetuity. It is made available under aCC-BY-NC-ND 4.0 International license.

treatment of advanced ovarian cancer, which could limit the progression of this poor prognosis cancer by ascites cancer cell dissemination.

Key words

PI3K signaling, tumour cell aggregation, resistance to treatment, signal-targeted therapies, malignant ascitis

40,858 characters

INTRODUCTION

Ovarian cancer is ranked in the world 8th in cancer incidence, but 4th in female mortality (1). It is often associated with a poor prognosis due to the frequent intraperitoneal implantation of tumour cells called peritoneal carcinomatosis observed at advanced stages (2,3). Found in about 89% of patients with a stade III or IV ovarian cancer, massive production of ascites fluid (inflammatory exudate present in peritoneal cavity) is in most cases associated with peritoneal carcinomatosis (4–6). Unlike most solid cancers, ovarian cancer cells rarely migrate haematogeneously but has the particularity to disseminate by direct extension to neighboring organs especially via the transcoelomic pathway. By this mechanism, cancer cells detach from the primary tumor and are then passively transported by the fluid throughout the peritoneal cavity in proximity of its entire wall composed of peritoneum and omentum, hence allowing the development of peritoneal carcinomatosis at multiple foci (2,3,7,8). Several cellular and molecular events are necessary before the establishment of peritoneal tumour implants resulting from transcoelomic migration of ovarian tumour cells: i) resistance to anoïkis, ii) transcoelomic dissemination facilitated by the flow of the peritoneal fluid , iii) escape of tumour cells to immune surveillance, iv) formation of spheroids or tumourospheres from aggregation of tumour cells in the ascites fluid, v) production of ascitic fluid as a vector of dissemination (2,3,7). Given the integrin repertoire expressed on the cell aggregates recovered from the patient ascites fluid, it is demonstrated that the cells then adhere to surfaces and implant within the peritoneum via the binding to the monolayer of mesothelial cells and to the extracellular matrix such as fibronectin and type I collagen (2,3,7).

Twenty years ago, peritoneal carcinomatosis was seen as an incurable pathology requiring palliative care only. However, the introduction of loco-regional therapies combining cytoreductive surgery with hyperthermic intraperitoneal chemotherapy (HIPEC) based on platinum salts or taxanes changed the management of this disease (9–11). Signal targeted therapies, such as those

bioRxiv preprint doi: https://doi.org/10.1101/777649; this version posted September 23, 2019. The copyright holder for this preprint (which was not certified by peer review) is the author/funder, who has granted bioRxiv a license to display the preprint in perpetuity. It is made available under aCC-BY-NC-ND 4.0 International license.

targeting PI3K (phosphoinositide 3-kinase) /Akt pathway, are currently tested in these patients with hopes of improvement of disease-free survival rates (12–14).

Tumour cell resistance to chemotherapy is now largely considered as enhanced in multicellular 3-dimensional (3D) structures. As an example, EMT-6 mammary tumour cells are more resistant to alkylating agents (Cyclophosphamide, Cisplatin, Thiotepa) when grown in 3D spheroids (2,15). Single or clustered cells can detach from breast or prostate primary tumours and can then be found in the bloodstream (16). Clusters of cells have an increased ability, as compared to single cells, to maintain cohesion and to survive once detached from breast primary tumours. Studying the formation of these aggregates and their resistance to treatment is also of major interest to improve understanding and therapeutic care of ovarian peritoneal carcinomatosis by targeting transcoelomic migration (16). In the peritoneal cavity, the formation and properties of these peritoneal tumoural aggregates are still poorly understood.

It is also largely accepted that microenvironment contributes to resistance to chemotherapy (17). Tumour stromal cells provide an environment promoting metastatic disease and resistance to treatments. Among microenvironment cells, mesenchymal stem cells (MSC) can be mobilized from bone marrow as well as from neighbouring organs at inflammation site resulting from tumour development, including in peritoneum (18,19). MSCs are a potential source of various cell types including tumour-associated fibroblasts (TAFs). MSC and TAFs have been shown to contribute to tumour cells' ability to form spheroids called tumourospheres under anchorage-independent culture conditions, increasing their capacity to induce tumour formation in vivo after mouse xenografts (20,21). The role of MSC in multicellular 3D culture of tumoural cells is poorly known.

The class I PI3K / Akt axis is one of the most commonly deregulated pathway in cancers, particularly in ovarian cancer, and could have a preponderant role in spheroids formation, as suggested by its involvement in regulation of the actin cytoskeleton (22–24). There are 4 isoforms of class I PI3K in Vertebrates: α, β, γ and δ. These heterodimeric enzymes are composed with a catalytic subunit called p110 associated with a regulatory subunit. PI3K activation results in the phosphorylation of phosphatidylinositol 4,5 biphosphate (PIP2) into phosphatidylinositol 3,4,5 triphosphate (PIP3) which acts as a second messenger in the cell. Downstream signals of PI3K, including the members of the Akt / mTOR (mammalian target of rapamycin) pathway, are numerous and involved in many cellular processes like cell cycle progression and actin cytoskeleton rearrangement (25–27). Activation of the PI3K pathway is associated with increased migration and invasion of different subpopulations of ovarian cancer cells, making this signaling pathway a predictor of invasive and migratory potential of ovarian tumour cells (28). Amongst the 4 class I PI3K encoding genes, *PIK3CA* gene encoding PI3Kα was found mutated in 6 to 33% of patients

bioRxiv preprint doi: https://doi.org/10.1101/777649; this version posted September 23, 2019. The copyright holder for this preprint (which was not certified by peer review) is the author/funder, who has granted bioRxiv a license to display the preprint in perpetuity. It is made available under aCC-BY-NC-ND 4.0 International license.

depending on the studies, and amplification or copy gain of this gene are found in 13 to 39.8% of the cases (29,30); these alterations are non-exclusive. Regarding the repartition of these alterations in the different subtypes of ovarian carcinomas, in high grade serous carcinomas, *PIK3CA* mutations are less frequent while amplifications are commonly found. The genetic landscape of ovarian carcinomas suggests that PI3K inhibitors, and in particular those targeting PI3Kα, could be tested in this pathology. Clinical trials with BYL719 (Alpelisib), a PI3Kα-selective inhibitor, in combination with estrogen receptor inhibitors already show clinical benefits with lower toxicity compared to the use of pan-PI3K inhibitors. BYL719 (Alpelisib) have just been approved for breast cancer (31,32), demonstrating the clinical interest of studying PI3K isoform-selective functions. The importance of PI3Kα activity in tumoural aggregates from ovarian origin is unknown.

This study objective is to validate a model of ovarian cancer cell aggregates and associated ascites, to demonstrate the involvement of PI3Kα during transcoelomic tumourosphere formation and their maintenance. For that purpose, we setup a 3D culture protocol allowing the formation of homotypic or heterotypic (with MSC) tumourospheres similar to tumour aggregates found in ovarian cancer ascites that we treated with PI3Kα-selective inhibitors. The use of these PI3K-targeting molecules is understudied in peritoneal carcinomatosis. Thus, our demonstration of a PI3Kα-driven formation of multi-cellular aggregates and their relation to mesenchymal stroma offers new therapeutic strategies to patients with peritoneal carcinomatosis.

RESULTS

Peritoneal tumour cells from ascites biopsies form aggregates which growth is delayed with high number of cells

Ascites are biopsied and are analysed to detect the presence of ovarian adenocarcinomatous cells. We first described the tumour cell aggregates found in ascites associated to ovarian adenocarcinomas in patients, which diagnostic was confirmed on cytospin and embedded preparation with routine coloration analysis with PAP, MGG, PAS and EpCAM IHC staining (Fig. 1A). The majority of the ascites (11/12 patients) were composed of isolated tumoural cells in limited amount with numerous aggregated tumoural cells (Fig. 1A). Only one case presented numerous isolated cells in association to aggregates. We observed a heterogeneity between patients in term of repartition of cellular aggregates, with patients with a high number of cell aggregates in ascites showing a better survival compared to patients with low aggregate number (Fig. 1B, Suppl. Table 1). When grown in 3D-favorable conditions, ascites cells formed dense spheroids (Fig. 1C). In order to better reproduce peritoneal carcinomatosis development of transcoelomic aggregates (Fig. 1D), we first developed a 3D culture system of peritoneal tumour cells derived from ovarian cancer

bioRxiv preprint doi: https://doi.org/10.1101/777649; this version posted September 23, 2019. The copyright holder for this preprint (which was not certified by peer review) is the author/funder, who has granted bioRxiv a license to display the preprint in perpetuity. It is made available under aCC-BY-NC-ND 4.0 International license.

SKOV-3 expressing GFP (Fig. 1E). After 14 days, we analysed the influence of cell numbers in aggregates and observed an increase of 75% and 13% of tumourosphere area when 5,000 and 10,000 cells were seeded respectively (Fig. 1F). Increase in number of initial cells appear to slow tumourosphere growth (Fig. 1E and F). Interestingly, area evolution (+24% in 7 days) (Fig. 1F) was correlated with expression of fluorescent GFP (+ 6% in 7 days) indicative of transcriptional/translational cellular activity (Fig. 1G, left), and metabolic activity indicative of cell survival (+ 29% in 7 days) (Fig. 1G right). We then carried out 3D cultures with 10,000 MSC and observed totally different aggregates evolution profiles compared to SKOV-3 cells with a very fast cell aggregation the day after seeding, and a more than 60% aggregate area decrease within 14 days compared to initial area (Suppl. Fig. 1A and B). We also observed fibrous-like structure formations within MSC aggregates whose nature remains to be determined (Suppl. Fig 1C). We then co-cultured 5000 GFP-expressing SKOV-3 cells with different quantities of Qdot-labeled MSCs (5, 50, 500 or 5000) as a model of stromal cells found in ascites and observed morphology, area and fluorescence localisation of these heterotypic tumourospheres (Fig. 1H and Suppl. Fig. 1D, E, F) (38). Heterotypic tumourosphere area decreased proportionally to the number of MSC with an apparent increased cohesion (Fig. 1H). On the other hand, GFP fluorescence corresponding to tumour cells did not vary regardless of MSC number, indicating that these cells induced a compaction of the tumourospheres without modifying tumour cell proliferation (Suppl. Fig. 1D and E). At a high ratio and 7 days after seeding, MSC cells clustered in the center of tumourospheres and colocalized with tumour cells (yellow staining, Suppl Fig. 1F).

Small sized tumourospheres show cellular growth and the addition of MSC to tumour cell spheroids results in increased compaction of the tumourospheres, reminiscent to what we observe with the formation of tumourospheres from patients' ascites cells.

PI3Kα inhibition prevents ovarian cancer cell tumourosphere formation.

The PI3K/Akt pathway plays a role in cell proliferation and survival but is also described as involved in the regulation of the actin cytoskeleton suggesting a role in tumourosphere formation (22,25–27). In order to determine the action of this pathway in the formation of SKOV-3 GFP multi-cellular aggregates, we treated them at seeding and 3 days later with PI3Kα-selective inhibitors A66 and BYL719 (Fig. 2A). We confirmed a concentration-dependent inhibition of Akt phosphorylation inhibition on S473 and T308 upon treatment with A66 and BYL719 (Fig. 2B-D), indicating 1- that PI3K pathway is constitutively activated in SKOV-3 cells, 2- that this activation is highly dependent on the PI3Kα isoform and 3- that the pharmacological agents used prevent its activity.

bioRxiv preprint doi: https://doi.org/10.1101/777649; this version posted September 23, 2019. The copyright holder for this preprint (which was not certified by peer review) is the author/funder, who has granted bioRxiv a license to display the preprint in perpetuity. It is made available under aCC-BY-NC-ND 4.0 International license.

We next compared the efficiency of a low (1µM) and medium (10µM) dose of PI3K inhibitors; in clinical trials, measured concentration of BYL719 in plasma are of the order of 50µM (39). After 4 and 7 days of treatment with 10 µM of BYL719, we observed a complete reduction of the tumourosphere area and a total loss of their fluorescence (Fig. 2E-G). Aggregates treated with 10 µM of A66 or 1 µM of BYL719 had comparable evolution profiles (Fig. 2E) with a decrease in tumourosphere area of about 30% compared to the control at d4 (Fig. 2F). We compared our results to the reference treatment of ovarian cancer, cisplatin, at doses found in patients (0.5µM and 5µM), 5µM being a dose close to toxicity in patients (40). A total disruption of SKOV-3 tumourospheres was observed only at high concentrations and after 7 days of treatment (Fig. 2H-J). Hence, we observed a significant alteration of tumourosphere cohesion, tumourosphere area (Fig. 2E-F) and cellular activity (Fig. 2G) at low doses of PI3Kα inhibitor, which was never seen in low doses of cisplatin (Fig. 2I-J). This effect is maintained in time.

These results suggest that PI3Kα inhibitors are able to reduce tumourosphere formation, while having a cytotoxic effect in a dose-dependent manner on these aggregated or non-aggregated cells whereas cisplatin appears to present only cytotoxic effect at high concentration close to patient toxicity dose and in a delayed manner.

PI3Kα selective inhibition prevents ovarian cancer cell tumourosphere maintenance.

In order to measure PI3Kα inhibitor effects on tumourosphere maintenance, we treated already established SKOV-3 GFP cell aggregates with PI3Kα inhibitors (A66 and BYL719) or cisplatin one day after tumourosphere formation and 3 days later (Fig. 3A). In order to test PI3Kα specificity of action amongst all PI3K isoforms on this mechanism, we also treated these tumourospheres with PI3Kβ (TGX-221) and PI3Kβ/δ inhibitors (AZD8186).

PI3Kα inhibitors caused a concentration-dependent tumourosphere area decrease and a tumourosphere morphology change corresponding to a decrease in compaction with maximal effect at day 7 (Fig. 3B-D). Used at 1 µM, treatment with BYL719 resulted in a greater effect than A66 with a significant decrease in tumourosphere area respectively of 86% and 43% as compared to the vehicle at day 7 (Fig. 3C, D), corresponding to a decrease in the initial size of tumourospheres. Treatment with TGX-221, a PI3Kβ-selective inhibitor, did not significantly modify the tumourophere morphology (Fig. 3B) or area (Fig. 3E) compared with vehicle treatment, with a tendency to an increase effect. AZD8186, a PI3Kβ/δ dual inhibitor, used at 1µM, only resulted in a significant decrease of 38% in tumourospheres area after 7 days of treatment, corresponding to an arrest in tumourosphere growth (Fig. 3F).

bioRxiv preprint doi: https://doi.org/10.1101/777649; this version posted September 23, 2019. The copyright holder for this preprint (which was not certified by peer review) is the author/funder, who has granted bioRxiv a license to display the preprint in perpetuity. It is made available under aCC-BY-NC-ND 4.0 International license.

A treatment with cisplatin reduced the tumourosphere area by 38% only after 7 days of treatment with a high concentration of 5 µM as compared to the vehicle at d7 (Fig. 3G-H), while 0.05 and 0.5µM did not prevent tumourosphere growth observed at d7.

PI3Kα inhibitors cause a decrease in the area of already established tumourospheres in an α isoform-specific manner.

Only PI3Kα inhibition impacts ovarian tumour cell viability in 3D culture.

We next aimed to determine the impact of the 3D culture on the tumour cell's resistance to the reference treatment of ovarian peritoneal carcinomatosis, cisplatin. We treated SKOV-3 GFP cells cultured in 2D or in 3D with PI3K inhibitors or cisplatin and evaluated the number of living cells with a MTT (2D) or Alamar Blue (3D) assay (Fig. 4A-E) and LIVE/DEAD assay (Fig. 4F-H)

In 2D, the two PI3Kα inhibitors showed a concentration-dependent cytotoxic effect on SKOV-3 GFP cells from a concentration of 1 µM (Fig. 4B). A significant decrease in living cell number was only observed for concentrations greater than or equal to 3.25 µM in cisplatin (Fig. 4C). In 3D, only PI3Kα specific inhibitors showed a cytotoxic effect on SKOV-3 tumourospheres at a high concentration of 10 µM (Fig. 4D). Cisplatin and PI3Kβ inhibitors did not modify the number of living cells in 3D (Fig. 4D and E).

Unlike cisplatin, PI3Kα inhibitors retained a concentration-dependent effect (although not significant) at d4 (Suppl. Fig. 2A and B). The cytotoxic effect of cisplatin observed in 2D was therefore abolished by 3D culture, whereas, albeit diminished, PI3Kα inhibitor treatment still showed cytotoxic effects in tumourospheres (Fig. 4B-E).

In order to further analyse organization and distribution of living and dead cells within tumourospheres under treatment, we labeled living cells in green (calcein) and dead cells in red (EthD-1). First, we found that when we analyse living cells, displayed in white, with their area quantified (Fig. 4 F-H), BYL-719 significantly decreased this marker of living cell (Fig. 4. G, H). SKOV-3 cell treatment with PI3Kα inhibitors caused an alteration in the tumourosphere cohesion and tended to increase dead cell amount (Suppl. Fig. 2C). Only 10 µM of BYL719 caused a significant decrease in living cell area (Fig. 4F and G). As observed previously, a 0.5 µM cisplatin concentration did not modify aggregates morphology. Tumourospheres disintegration and living cell surface decrease was only detected after 7 days with 5 µM of platinum salt treatment (Fig. 4F and H). As observed before, PI3Kα inhibitors induced a rapid decrease of tumourosphere cohesion and viability (Fig. 4F and G, Suppl. Fig. 2) compared to cisplatin which was followed by a tumourosphere disintegration only at high concentration after 7 days of treatment (Fig. 4F and H).

bioRxiv preprint doi: https://doi.org/10.1101/777649; this version posted September 23, 2019. The copyright holder for this preprint (which was not certified by peer review) is the author/funder, who has granted bioRxiv a license to display the preprint in perpetuity. It is made available under aCC-BY-NC-ND 4.0 International license.

Regarding the localization of living and dead cells, untreated SKOV-3 tumourospheres appeared to have a dead cell inner core, while treatment with PI3Kα inhibitors suppressed this core, with a staining spread on the whole area of the tumourosphere, in particular in the outer layer of the tumourosphere (Suppl. Fig. 2C). As observed before, the PI3Kβ specific inhibitor TGX-221 at 1µM did not alter SKOV-3 WT tumourospheres morphology (Fig. 4F) and area (Fig. 4G). At high concentration, concentration at which the selectivity towards PI3Kβ and class PI3Ks is not demonstrated, we observed an unexplained increased area of living cells despite a loss of cohesion (Fig. 4F), combined with decreased number of inner dead cells in comparison to other PI3Kβ-targeting inhibitors at similar drug concentration (Suppl. Fig. 2C). AZD8186 only slightly modified living cells area (Fig. 4G) but seemed to alter the tumourosphere morphology by altering their cohesion at both concentrations (Fig. 4F).

Despite a decreased effect in 3D culture, PI3Kα inhibitor is shown as the most effective treatment as compared to the conventional treatment.

PI3K inhibitors decrease tumourosphere survival in presence of cisplatin.

If used in the clinic for the treatment of ovarian cancer, inhibitors of PI3K will be tested in combination (39). SKOV-3 cells were cultured in 3D similarly to previous experiments and treated with a combination of treatments associating a fixed 1 µM concentration of PI3K inhibitors with increased concentrations of cisplatin. The tumourosphere area, the metabolic activity and the surface of living cells were quantified (Fig. 5).

Combination of low concentration of cisplatin with PI3Kα inhibitors appeared to alter more efficiently SKOV-3 GFP tumourospheres morphology compared to control (cisplatin alone) but not significantly more than the corresponding inhibitor alone (Fig. 5A et B). These results were confirmed by measurements of tumourosphere area (Fig. 5C) and of the area of calcein positive alive cells (Fig. 5E). However, albeit non-significant, the metabolic activity tended to decrease only with the combination of therapeutic agents (Cisplatin with A66, BYL-719, TGX-221, AZD8186), in particular with α-selective inhibitors (Fig. 5D). Moreover, a greater effect of the combination cisplatin low dose and PI3Kα inhibitors on decreasing the area of metabolically active cells seemed to be observed compared with the condition cisplatin 5 µM (Fig. 5E). Results obtained with combination of cisplatin with TGX-221 and AZD8186 were not significantly changed neither for area nor for living cell numbers in the SKOV-3 GFP tumourospheres as compared to cisplatin alone.

bioRxiv preprint doi: https://doi.org/10.1101/777649; this version posted September 23, 2019. The copyright holder for this preprint (which was not certified by peer review) is the author/funder, who has granted bioRxiv a license to display the preprint in perpetuity. It is made available under aCC-BY-NC-ND 4.0 International license.

Differences in the effects observed with the three different assays show that the key combined action of PI3Kα inactivation and cisplatin treatment consists in decreasing cell survival upon tumourosphere dissociation.

Finally, addition of MSC which compacted the tumourosphere tended to decrease the efficiency of PI3Kα inhibitors on tumourosphere area but they always seemed to have an effect (Fig. 6A and B). The absence of direct effect of all PI3K inhibitors on MSC was verified (Suppl. Fig. 3).

In conclusion, the combination therapy of PI3Kα with cisplatin leads to tumourosphere survival decrease possibly via a dissociation of the tumour cell aggregate.

DISCUSSION

Because of a frequent late diagnosis, ovarian cancers associated with peritoneal carcinomatosis most often develop ascites. This metastatic process involves a transcoelomic migration step requiring tumour cell aggregation within the peritoneal cavity. This three-dimensional structure allows tumour cells to better survive to conventional chemotherapies (2,41). The current therapeutic arsenal lacks treatments targeting the metastatic disease, which represents a major public health issue due to its morbidity and mortality. To date, HIPEC has therapeutic interest in peritoneal carcinomatosis treatment but remains poorly practiced because of the potential toxicities (42–46). Our data demonstrate that PI3Kα should be added to their therapeutic arsenal.

We found tumor aggregates in all the ovarian cancer patients' ascites we studied. Surprisingly, patients with a high number of cell aggregates showed a better survival than patients with low aggregate number (Fig. 1A-C). These clinical observations reinforce the need to better understand ovarian tumor cell aggregate formation.

In this study, we developed a 3D culture method to better mimic the aggregate formation observed within the ascites fluid and responsible for short term peritoneal carcinomatosis. We used ovarian tumour cells SKOV-3 coming from ascites and realized tumourospheres in round-bottomed plates treated to prevent cell adhesion (47). After only a few hours, ovarian tumour cells form round or elliptical structures typically corresponding to those described in the literature (48), reproduced as well with 3D culture of patients (Fig. 1C). SKOV-3 tumourospheres area increases over time and most of the cells composing the core of the tumourosphere are dead (Suppl. Fig. 2C) similar to observations of other teams (49,50). However, cell density and GFP fluorescence do not significantly vary over time indicating a stability in the cell number composing the tumourospheres (Fig. 1E, G).

bioRxiv preprint doi: https://doi.org/10.1101/777649; this version posted September 23, 2019. The copyright holder for this preprint (which was not certified by peer review) is the author/funder, who has granted bioRxiv a license to display the preprint in perpetuity. It is made available under aCC-BY-NC-ND 4.0 International license.

PI3K, and more particularly the α isoform, play a role in the rearrangement of the actin cytoskeleton (22,51). Actin involvement in migration and invasion is no longer to be proven and, according to our hypothesis, PI3Kα would facilitate ovarian tumour cell aggregate formation (25–27). In order to validate this hypothesis, we treated SKOV-3 cells tumourospheres during seeding with different concentrations of PI3Kα inhibitors, A66 (33) and BYL719 (34). After treatment of these aggregates, and regardless of concentration used, we observe in microscopy sphere disorganization up to complete disintegration for 10µM of BYL719 treatment. Assessment of cytotoxicity was carried out in parallel on these tumourospheres. As an example, BYL719 at 1 µM concentration decreases aggregate area of 29.1% but only decreases of 8.9% in living cells percentage after 7 days. The fact that the treatment is carried out at the seeding time and that the morphology modifications are observed in a short time show that this disorganization is not only a result of an inhibitor cytotoxicity with regard to percentages of remaining viable cells obtained.

Because most of the patients with ovarian cancer already present ascites fluid containing cell aggregates at the initiation of the treatment (52), we sought to determine the role of PI3K on the maintenance of existing tumour aggregates. We treated our tumourospheres the day after seeding. While a treatment with 10 µM of BYL719 during cell seeding causes a total reduction in measurable sphere area after 7 days, the same treatment started one day later results in a 68.5% reduction in sphere area. This efficacy reduction observed after PI3Kα inhibitor treatment could be due to a lack of treatment penetration within the spheres (53). PI3Kα seems to have a role in both formation and maintenance of ovarian tumour cell aggregates.

Here, SKOV-3 cells cultured in 3D show a 33.4% increase in resistance to 10 µM of BYL719 treatment compared to a 2D culture. Resistance to cisplatin, a standard treatment in HIPEC for ovarian cancer, is increased by approximately 70% by this 3D culture (Fig. 4). It has been repeatedly demonstrated that 2D cytotoxicity studies do not account for complete tissue physiology and overestimate the cytotoxic potential of the tested molecules (15,54). Aggregate formation study has led to the discovery of multicellular resistance existence and has demonstrated protection of ovarian carcinoma cells against apoptosis induced by cisplatin. In a 3D culture, these cells are 18, 15 or 58 times more resistant to cisplatin at 25, 50 and 100 µM respectively (15). In addition, proliferation within the spheres decreases in comparison with cells cultured in 2D, partially explaining these cells escape to such treatments induced death targeting cells in replication (15,55). The comparison of our 2D and 3D cytotoxicity results accounts for the same type of resistance for SKOV-3 GFP cells to that observed in the literature. Inhibitors seem to maintain a concentration-dependent effect at day 4 compared to cisplatin, which at this stage is ineffective (Suppl. Fig. 2A

bioRxiv preprint doi: https://doi.org/10.1101/777649; this version posted September 23, 2019. The copyright holder for this preprint (which was not certified by peer review) is the author/funder, who has granted bioRxiv a license to display the preprint in perpetuity. It is made available under aCC-BY-NC-ND 4.0 International license.

and B), suggesting that inhibitors retain an earlier action on tumourosphere cohesion, compared with cisplatin.

Whatever the timing of treatment, cisplatin has a significant effect only at a high concentration of 5 µM (Fig. 2I and 3H). As for PI3K inhibitors, cisplatin has a lesser efficacy when used the day after seeding compared to a treatment during cell seeding. In addition, in 3D, PI3Kα inhibitors induce a quicker effect than cisplatin. BYL719 leads to a significant reduction of the area parameter at low concentration of 0.1 µM (Fig. 3D) which allows us to consider an effect on peritoneal carcinomatosis while maintaining a low toxicity.

We also conducted these experiments with PI3Kβ inhibitors, TGX-221 (35) and AZD8186 (36). TGX-221 has no significant effect on either sphere area or metabolism (Fig. 3E and 4D). On the other hand, AZD8186 induces a significant decrease of tumourosphere area at high concentration which could be due to its action of PI3Kα. Indeed, PI3Kα IC50 of A66 are similar (32 and 35 nM respectively) (Fig. 3E and 4D) (36). Overall, we show that the maximum effects on tumourosphere area are obtained with PI3Kα inhibitors, showing a specificity of action of this isoform.

Our hypothesis that PI3Kα acts on spheroid development seems to be verified by the experiments carried out in this study. PI3Kα action on actin cytoskeleton could be the source of this effect on spheroids (27,56). This hypothesis is reinforced by the knowledge of existing link between the polymerized actin and the adhesive molecules such as E or P cadherins. P-cadherin expression promotes migratory potential and aggregation of circulating ovarian cancer cells into multicellular aggregates (57). These elements highlighting actin role could in part explain PI3Kα involvement in cell clustering (58,59).

Intercellular interactions between two same cell types have a role in metastatic disease development. By serial intraperitoneal injection of green and red fluorescent cells, newly introduced cancer cells have been shown to adhere preferentially to existing tumours (60). Therapies targeting adhesion between cancer cells of the same type, such as PI3Kα inhibitors, are worthy of consideration for improving peritoneal carcinomatosis management. Tumour aggregate disorganization induced by PI3Kα inhibitors would allow a better cisplatin bioavailability within the tumourospheres by breaking decreasing gradient of diffusion from the periphery to the center of these 3D structures (61). Another hypothesis for increased efficiency of cisplatin upon PI3Kα inactivation could be that tumourosphere dissociation decreases the solid stress that build up in the 3D culture (62) and with increase liquid pressure (63) or the shear stress caused by ascites fluid motion in the peritoneal cavity (8), or the tensile stress caused by MSC, releasing the proliferation rate and allow cisplatin to function. This remains to be demonstrated in follow-up studies.

bioRxiv preprint doi: https://doi.org/10.1101/777649; this version posted September 23, 2019. The copyright holder for this preprint (which was not certified by peer review) is the author/funder, who has granted bioRxiv a license to display the preprint in perpetuity. It is made available under aCC-BY-NC-ND 4.0 International license.

One parameter that we find key to patient prognosis is the tumour aggregate size. This could account for the heterogeneity of treatment response of patients with chemotherapeutic agents. Others also found that forming spheroids of small size is more relevant to patient disease (64). If compression, interstitial pressure, tension increase invasion features through epithelial-to-mesenchymal transdifferentiation (EMT) (62,63), our clinical data demonstrate that less aggressive cells tend to grow in larger multicellular aggregates which could decrease their proliferation rate and increase their death ratio. Finding molecular determinant of such behavior could be of interest to understand the progression of ovarian cancer. Indeed, others found that morphology of human donor ascites aggregates is conserved in tumour-bearing mice injected by i.p. with these cells (38).

In conclusion, our results show that isolated cells obtained from small tumour aggregates can be treated with PI3Kα inhibitors. This is all the more important given that we find that patients with smaller aggregates presented a poorer prognosis. These dissociated cells are shown to be more sensitive to conventional therapies (15,54) and PI3K-driven tumour cell aggregate dissociation demonstrates the potential interest of PI3Kα inhibitors in combination therapy with this type of chemotherapy. Hence, our results that demonstrate the crucial role of PI3Kα in the formation and maintenance of ovarian tumour cells aggregates, make this enzyme a therapeutic target of interest for peritoneal carcinomatosis treatment (Fig. 7). Indeed, the use of an intraperitoneal PI3Kα inhibitor pretreatment separating aggregates into individual cells will allow the sensitization of tumourospheres to the treatments used in HIPEC and constitutes a promising alternative to improve management of a pathology with a very poor prognosis.

MATERIAL AND METHODS

Patient ascites-derived cell tumourospheres

Ascites' fluids are taken from patients with ovarian cancer after consent (CRB Cancer des Hôpitaux de Toulouse, IUCT-O, Toulouse – BB-0033-00014, DC-2008-463, AC-2013-1955). Information on patients are detailed in Supplementary Table 1, clinical and biological annotations of the samples have been declared to the CNIL (Comité National Informatique et Libertés). For diagnosis purposes, fluids are analysed on cytospins. Following the biopsy, the aspirated material is sent without any fixation rapidly to our laboratory in an EDTA tube at 4°C. Before any process, the mononucleated cells including white blood cell (wbc) and the red blood cells (rbc) are counted on a malassez slide. The cell number is given by µl. The mononucleated cell count will determine the dilution necessary to prepare an adequate cytospin. An aliquot of 200 µl of the sample diluted to 500 mononucleated cells/µl is cytocentrifuged on a slide (700 rotations per minute corresponding to 55 g /min 8 min on Shandon cytospin 4 centrifuge). Routine coloration is then achieved using

bioRxiv preprint doi: https://doi.org/10.1101/777649; this version posted September 23, 2019. The copyright holder for this preprint (which was not certified by peer review) is the author/funder, who has granted bioRxiv a license to display the preprint in perpetuity. It is made available under aCC-BY-NC-ND 4.0 International license.

May Grunwald Giemsa (MGG), Papanicolaou (PAP) and Periodic acid–Schiff stains (PAS) (Fig. 1A). Microscopic examination of the colored slides allows to establish a formula indicating the percentage of the different mononucleated cells and the detection of carcinomatous cell. The number of aggregates on the cytospin spot and the number of cells in the aggregates is noted as well as the aggregate density (Fig. 1A, top). A normalized aggregate number has been determined by multiplying these two parameters. Rich aggregates ascites have a normalized aggregates number above 100,000 while poor aggregates ascites have a normalized aggregates number below 100,000. To assure malignancy, immunocytochemistry is performed with EpCam (clone Ber-EP4 IVD 05435676001 Ventana Roche). The cytospin cell preparation is fixed 10 min in preservCyt solution (Cytyc Corporation, Marlborough, Mass) at room temperature and processed in an automated staining plateform (Ventana bench mark Ultra). After primary antibody incubation, the detection used is Ultra view Dab (VENTANA roche) (Fig. 1A, bottom). Cells contained in the fluid are counted with Cellometer® then seeded in DMEM (Dulbecco's Modified Eagle's Medium, Sigma) in round bottom 96 well plates (Nunclon Sphera, ThermoFisher Scientific) at 5,000 cells per well. The culture medium is supplemented with 10% FCS (fetal calf serum), 1% L-glutamine, 1% penicillin-streptomycin and 0.01% plasmocin (Invitrogen).

Cell lines and culture conditions

SKOV-3 WT cells are peritoneal tumour cells originating from ascites of ovarian cancer and present the following genetic alterations: *PIK3CA H1047R*; *TP53* copy loss. SKOV-3 GFP cells correspond to genetically modified SKOV-3 WT cells expressing GFP (Green Fluorescent Protein). MSCs (Mesenchymal Stem Cells) are derived from healthy donors who underwent hip surgery (Etablissement Français du Sang).

Cells are cultured at 37°C, 5% CO2 under humid atmosphere, in RPMI 1640 medium (Roswell Park Memorial Institute medium, Sigma) for SKOV-3 cells and DMEM (Dulbecco's Modified Eagle's Medium, Sigma) for MSC and 50% of each medium is used when two cells type are mixed. The culture medium is supplemented with 10% FCS (fetal calf serum), 1% L-glutamine, 1% penicillin-streptomycin and 0.01% plasmocin (Invitrogen).

Pharmacological inhibitors

Pharmacological inhibitors used in this study are as follow : A66 (Axon Medchem) PI3Kα inhibitor (in vitro IC50 in nM: p110α: 32; β: >12500; δ: >1250; γ: 3480) (33); BYL719 (Apex Bio) PI3Kα inhibitor (in vitro IC50 in nM: p110α: 4.6; β: 1156; δ: 290; γ: 250) (34); TGX-221 (Axon Medchem) PI3Kβ inhibitor (in vitro IC50 in nM: p110α: 5000; β: 5; δ: 100; γ: 10000) (35);

bioRxiv preprint doi: https://doi.org/10.1101/777649; this version posted September 23, 2019. The copyright holder for this preprint (which was not certified by peer review) is the author/funder, who has granted bioRxiv a license to display the preprint in perpetuity. It is made available under aCC-BY-NC-ND 4.0 International license.

AZD8186 (MedChemExpress) PI3Kβ/δ inhibitor (in vitro IC50 in nM: p110α: 35; β: 4; δ: 12; γ: 675) (36).

Living cell assay assessed by mitochondrial reductase activity assay in 2D (MTT)

One thousand patient-derived tumoural cells or SKOV-3-GFP and SKOV-3-WT cells, with or without increasing amount of MSC cells are seeded in 96-well plates. The following day, cells are treated with specific inhibitors of PI3Kα, A66, BYL719 at increasing concentrations of 0.01 to 10 µM with 1/10 intermediate dilutions (control condition (vehicle) comprising 0.1% of DMSO) or with Cisplatin (kindly supplied by the Toulouse University Institute of Cancer's pharmacy, IUCT-O) at increasing concentrations of 0.05 to 100 µM with intermediate 1/2 dilutions. After 72 hours of treatment, the number of living cells is quantified by MTT colorimetric test. The mean value obtained for each condition is related to the control (untreated condition for Cisplatin and vehicle for PI3K inhibitors).

Tumourosphere culture, area quantification and living cell assay assessed by cytosolic and mitochondrial reductase activity assay in 3D (Alamar blue)

SKOV-3 WT and GFP cells are suspended in a complete RPMI medium containing or not 5% methylcellulose (Sigma Aldrich). Cells are seeded in round bottom 96 well plates (Nunclon Sphera, ThermoFisher Scientific) at 5,000 cells per well. The plates are then maintained at 37°C, 5% CO2 under a humid atmosphere. For heterotypic 3D culture, a cell suspension comprising a mixture of 5,000 SKOV-3 WT tumour cells and 5, 50, 500 or 5,000 MSC (previously labeled with quantum dots) is seeded into triplicates in 96-well round bottom plates (Nunclon Sphera, ThermoFisher Scientific) in an equivolumic solution of DMEM and RPMI medium. Cell clusters are treated at seeding or 24h after, with A66 or BYL719, TGX-221 or AZD8186 at 1 or 10 µM in association or not with cisplatin at 0.5, 5 or 50 µM with their respective vehicle controls. Cell clusters obtained are observed and imaged under AxioVert microscope on d1, d4, d7, d10, and d14 using the ZEN® software (Carl Zeiss). Their diameter and surface are measured using the same software. For each conditions, triplicates are performed and average of area values are related to d1 average of the corresponding experiment (representing 100% of the surface). In parallel, at the end of d0, d3 and d6 treatment, the living cells are quantified by colorimetric assay using the Alamar Blue™ cell viability reagent (Invitrogen). Average absorbance is reported to the control on the day of measurement (representing 100% of living cells). To set up the conditions, we seeded 5,000 or 10,000 SKOV-3 GFP cells in round-bottom plates treated to enhance cell aggregation and measured by microscopy the evolution of area of tumourospheres thus formed. Of note, addition of methylcellulose (MC) (cellulose polysaccharide derivative promoting cell suspension by making

bioRxiv preprint doi: https://doi.org/10.1101/777649; this version posted September 23, 2019. The copyright holder for this preprint (which was not certified by peer review) is the author/funder, who has granted bioRxiv a license to display the preprint in perpetuity. It is made available under aCC-BY-NC-ND 4.0 International license.

medium more dense and viscous) in the culture medium did not improve tumourosphere formation (not shown), as opposed to data described in (37). MC seems to delay, by about 4 days, the aggregation of SKOV-3 GFP cells (not shown). Plate centrifugation (one minute at 300g) did not bring any modification to tumour aggregates formation either (not shown).

Qdot® Cell labelling of MSC cells

The labelling is performed according to the supplier's recommendations; in details, the equimolar mix of the labelling kit at dilution 1/100 is incubated for 1 hour at room temperature and is then applied directly to the cell cultures. This is followed by a 45 min incubation at 37° C, 5% CO2 under a humid atmosphere. Labeled cells are then washed twice with complete growth medium.

Assessment of cell viability with LIVE/DEAD® cytotoxicity assay in 3D

SKOV-3 WT cell tumourospheres are cultured and treated as described previously. On d1, d3 and d7, live (in green) and dead (in red) cells are labeled using the LIVE/DEAD® kit (ThermoFisher Scientific) containing approximately 2 µM calcein and 4 µM EthD-1. After 1 hour of ambient temperature incubation, clusters obtained are photographed using ZEN® software. Area occupied by living cells is quantified using the ImageJ® software. Means are related to the control of the corresponding day (representing 100% of living cells).

Western Blot

SKOV-3 GFP cells are seeded at 80% confluency and then deprived of serum overnight. The day after, cells are pre-treated with PI3Kα inhibitors (A66 and BYL719) at 0.01, 0.1, 1 and 10 µM for 1 hour. Cells are then supplemented with 10% FCS for 15 minutes without changing the medium, washed twice with cold PBS then lysed on ice in lysis buffer (150mM NaCl, 1mM EDTA, 50mM Tris HCl, 1% Triton, 1mM DTT, 2mM NaF, 2mM Na_3VO_4, supplemented with a cocktail of proteases inhibitors "complete Mini EDTA-free" Roche®). Protein concentration is determined with the BCA assay (BiCinchoninic Acid assay, Interchim®).

Fifty micrograms of protein are separated on a 8% or 12% polyacrylamide gel under constant voltage (90V) in denaturing conditions in a migration buffer (25mM Tris Base, 192mM glycine, 1% SDS) and transferred to Nitrocellulose 0.45µm (Whatman®) in semi-dry phase for 30 minutes thanks to the Transblot Turbo system (Bio-Rad®) in a transfer buffer (25mM Tris, 192mM glycine, 0.5% SDS, 20% absolute Ethanol). Membranes are saturated in TBS-T (Tris Buffer Saline, 10mM Tris-HCl pH 7.4, 150mM NaCl, 0.05% Tween) 5% skimmed milk for 45 min at room temperature. There are then incubated with the primary antibody diluted in TBS-T/5% BSA (Bovine

bioRxiv preprint doi: https://doi.org/10.1101/777649; this version posted September 23, 2019. The copyright holder for this preprint (which was not certified by peer review) is the author/funder, who has granted bioRxiv a license to display the preprint in perpetuity. It is made available under aCC-BY-NC-ND 4.0 International license.

Serum Albumin) containing 0.01% Na Azide overnight at 4°C as described below. Membranes are washed 3 times for 10 minutes with TBS-T and then incubated in a TBST/milk 5% solution containing secondary antibody (ThermoFisher Scientific) coupled to HRP (Horse Raddish Peroxidase) for 1h30. Membranes are washed 3 times for 10 min with TBS-T then, specific bands are revealed in darkroom after the membrane incubation with ECL reagent RevelBlot® Plus-chemiluminescent substrate of HRP for 5 min. Proteins are quantified using the ImageJ software and correspond to two independent experiments.

Primary antibody	Origin	Dilution	Provider	Size	Secondary antibody
pAkt (S473)	Rabbit	1/1000	Cell signaling #4060	60kDa	1/3300
pAkt (T308)	Rabbit	1/1000	Cell signaling #4056	60kDa	1/3300
Akt total	Rabbit	1/1000	Cell signaling #4691	60kDa	1/20 000
pCofilin (S3)	Rabbit	1/1000	Cell signaling #3313	19kDa	1/3300
Cofilin	Rabbit	1/1000	Cell signaling #5175	19kDa	1/20000
β-Actine	Mouse	1/2000	Sigma Aldrich AC74	42kDa	1/10 000

Statistics

Quantitative variables were presented by means and qualitative data by percentages. Group comparisons were made using the ANOVA test (matched data) and Student's t test for parametric tests. For all this study, a statistical difference is reached for $p < 0.05$ (*), $p < 0.01$ (**), or $p < 0.001$ (***).

Acknowledgments

We thank all members of SigDYN for their comments during the writing of the manuscript, CRCT core technology platform in particular Laetitia Ligat for imaging, Marie Veronique Joubert for her help in MSC culture. JGG's laboratory belongs to Toucan, Laboratoire d'Excellence, ANR, an integrated research program on Signal-targeted Drug Resistance. JGG's laboratory for this topic was/is funded by ARC (PJA20171206596), Toucan ANR Laboratory of Excellence, Fondation de France (salary to BT), Hopitaux de Toulouse (salary to AT).

Author contribution

All authors have seen and approved the manuscript, analysed the results and contributed to the conceptual advance proposed by the results. JGG conceived the project. AT, BT conceived, planned and performed experiments. BT and JGG supervised AT for the experimental settings, data analysis and manuscript writing with input from CB. CB supervised the ethical

bioRxiv preprint doi: https://doi.org/10.1101/777649; this version posted September 23, 2019. The copyright holder for this preprint (which was not certified by peer review) is the author/funder, who has granted bioRxiv a license to display the preprint in perpetuity. It is made available under aCC-BY-NC-ND 4.0 International license.

authorisations linked with patients, provided human samples and all data and analysis related to human patients. AT, BT and JGG wrote the article with input from CB.

Conflict of interest

The authors have no conflict of interest to declare.

The paper explained

PROBLEM

Malignant serous effusions are characterized by the presence of neoplastic cells in the increased serous fluid and are a common manifestation of metastatic disease. The detection of these cells is important as it is a marker of tumor progression and is associated with shorter survival. In these fluids that are simply sampled by needle biopsy, tumour cells are in suspension, aggregate in 3D structures and are passively disseminated in the cavity. Because tumour cell resistance to chemotherapy is now largely considered as enhanced in multicellular 3D structures, we questioned if this clinical situation could explain persistence of tumour cells upon treatment and participate to therapy resistance.

RESULTS

We focused on ovarian cancer clinical situation, where more than a third of patients present tumour cells in their peritoneal cavity, in a liquid that is called ascites. We found that the size of the tumour aggregates influenced positively the prognosis of the patients and that dissociation of the tumour aggregates led to an increased sensitivity to therapies. The protumourigenic signalling driven by PI3Kα, one of the gene the most mutated in cancers, by promoting compaction of small sized tumour aggregates favoured therapy resistance. The clinically approved therapies that target PI3Kα decreased the survival of ovarian cancer cells from ascites.

CLINICAL IMPACT

We hence identified a signaling pathway of interest for the treatment of advanced ovarian cancer, which could limit the progression of this poor prognosis cancer by ascites cancer cell dissemination.

References

bioRxiv preprint doi: https://doi.org/10.1101/777649; this version posted September 23, 2019. The copyright holder for this preprint (which was not certified by peer review) is the author/funder, who has granted bioRxiv a license to display the preprint in perpetuity. It is made available under aCC-BY-NC-ND 4.0 International license.

1. Jemal A, Bray F, Center MM, Ferlay J, Ward E, Forman D. Global cancer statistics. CA Cancer J Clin. mars 2011;61(2):69‑90.

2. Tan DSP, Agarwal R, Kaye SB. Mechanisms of transcoelomic metastasis in ovarian cancer. Lancet Oncol. nov 2006;7(11):925‑34.

3. Yin M, Li X, Tan S, Zhou HJ, Ji W, Bellone S, et al. Tumor-associated macrophages drive spheroid formation during early transcoelomic metastasis of ovarian cancer. J Clin Invest. 10 oct 2016;126(11):4157‑73.

4. Thomassen I, Lemmens VEPP, Nienhuijs SW, Luyer MD, Klaver YL, de Hingh IHJT. Incidence, Prognosis, and Possible Treatment Strategies of Peritoneal Carcinomatosis of Pancreatic Origin: A Population-Based Study. Pancreas. janv 2013;42(1):72‑5.

5. Heintz APM, Odicino F, Maisonneuve P, Quinn MA, Benedet JL, Creasman WT, et al. Carcinoma of the ovary. FIGO 26th Annual Report on the Results of Treatment in Gynecological Cancer. Int J Gynaecol Obstet Off Organ Int Fed Gynaecol Obstet. nov 2006;95 Suppl 1:S161-192.

6. Cerne K, Kobal B. Ascites in Advanced Ovarian Cancer. In: Devaja O, Papadopoulos A, éditeurs. Ovarian Cancer - From Pathogenesis to Treatment [Internet]. InTech; 2018 [cité 16 sept 2019]. Disponible sur: http://www.intechopen.com/books/ovarian-cancer-from-pathogenesis-to-treatment/ascites-in-advanced-ovarian-cancer

7. Lengyel E. Ovarian Cancer Development and Metastasis. Am J Pathol. sept 2010;177(3):1053‑64.

8. Rizvi I, Gurkan UA, Tasoglu S, Alagic N, Celli JP, Mensah LB, et al. Flow induces epithelial-mesenchymal transition, cellular heterogeneity and biomarker modulation in 3D ovarian cancer nodules. Proc Natl Acad Sci. 28 mai 2013;110(22):E1974‑83.

9. Wright AA, Cronin A, Milne DE, Bookman MA, Burger RA, Cohn DE, et al. Use and Effectiveness of Intraperitoneal Chemotherapy for Treatment of Ovarian Cancer. J Clin Oncol. 10 sept 2015;33(26):2841‑7.

10. Ansaloni L, Coccolini F, Morosi L, Ballerini A, Ceresoli M, Grosso G, et al. Pharmacokinetics of concomitant cisplatin and paclitaxel administered by hyperthermic intraperitoneal chemotherapy to patients with peritoneal carcinomatosis from epithelial ovarian cancer. Br J Cancer. janv 2015;112(2):306‑12.

11. Bakrin N, Bereder JM, Decullier E, Classe JM, Msika S, Lorimier G, et al. Peritoneal carcinomatosis treated with cytoreductive surgery and Hyperthermic Intraperitoneal Chemotherapy (HIPEC) for advanced ovarian carcinoma: A French multicentre retrospective cohort study of 566 patients. Eur J Surg Oncol EJSO. déc 2013;39(12):1435‑43.

12. Mabuchi S, Kuroda H, Takahashi R, Sasano T. The PI3K/AKT/mTOR pathway as a therapeutic target in ovarian cancer. Gynecol Oncol. avr 2015;137(1):173‑9.

13. Cheaib B, Auguste A, Leary A. The PI3K/Akt/mTOR pathway in ovarian cancer: therapeutic opportunities and challenges. Chin J Cancer. 5 janv 2015;34(1):4‑16.

bioRxiv preprint doi: https://doi.org/10.1101/777649; this version posted September 23, 2019. The copyright holder for this preprint (which was not certified by peer review) is the author/funder, who has granted bioRxiv a license to display the preprint in perpetuity. It is made available under aCC-BY-NC-ND 4.0 International license.

14. Bedard PL, Tabernero J, Janku F, Wainberg ZA, Paz-Ares L, Vansteenkiste J, et al. A Phase Ib Dose-Escalation Study of the Oral Pan-PI3K Inhibitor Buparlisib (BKM120) in Combination with the Oral MEK1/2 Inhibitor Trametinib (GSK1120212) in Patients with Selected Advanced Solid Tumors. Clin Cancer Res. 15 févr 2015;21(4):730‑8.

15. Kobayashi H, Man S, Graham CH, Kapitain SJ, Teicher BA, Kerbel RS. Acquired multicellular-mediated resistance to alkylating agents in cancer. Proc Natl Acad Sci U S A. 15 avr 1993;90(8):3294‑8.

16. Aceto N, Bardia A, Miyamoto DT, Donaldson MC, Wittner BS, Spencer JA, et al. Circulating tumor cell clusters are oligoclonal precursors of breast cancer metastasis. Cell. 28 août 2014;158(5):1110‑22.

17. Castells M, Thibault B, Delord J-P, Couderc B. Implication of Tumor Microenvironment in Chemoresistance: Tumor-Associated Stromal Cells Protect Tumor Cells from Cell Death. Int J Mol Sci. 30 juill 2012;13(8):9545‑71.

18. Karnoub AE, Dash AB, Vo AP, Sullivan A, Brooks MW, Bell GW, et al. Mesenchymal stem cells within tumour stroma promote breast cancer metastasis. Nature. oct 2007;449(7162):557‑63.

19. Komarova S, Kawakami Y, Stoff-Khalili MA, Curiel DT, Pereboeva L. Mesenchymal progenitor cells as cellular vehicles for delivery of oncolytic adenoviruses. Mol Cancer Ther. mars 2006;5(3):755‑66.

20. Lee J-H, Kim S-K, Khawar IA, Jeong S-Y, Chung S, Kuh H-J. Microfluidic co-culture of pancreatic tumor spheroids with stellate cells as a novel 3D model for investigation of stroma-mediated cell motility and drug resistance. J Exp Clin Cancer Res [Internet]. déc 2018 [cité 21 janv 2018];37(1). Disponible sur: https://jeccr.biomedcentral.com/articles/10.1186/s13046-017-0654-6

21. Kabashima-Niibe A, Higuchi H, Takaishi H, Masugi Y, Matsuzaki Y, Mabuchi Y, et al. Mesenchymal stem cells regulate epithelial-mesenchymal transition and tumor progression of pancreatic cancer cells. Cancer Sci. févr 2013;104(2):157‑64.

22. Baer R, Cintas C, Dufresne M, Cassant-Sourdy S, Schönhuber N, Planque L, et al. Pancreatic cell plasticity and cancer initiation induced by oncogenic Kras is completely dependent on wild-type PI 3-kinase p110α. Genes Dev. 1 déc 2014;28(23):2621‑35.

23. Huang J, Zhang L, Greshock J, Colligon TA, Wang Y, Ward R, et al. Frequent genetic abnormalities of the PI3K/AKT pathway in primary ovarian cancer predict patient outcome. Genes Chromosomes Cancer. août 2011;50(8):606‑18.

24. Zhang Y, Kwok-Shing Ng P, Kucherlapati M, Chen F, Liu Y, Tsang YH, et al. A Pan-Cancer Proteogenomic Atlas of PI3K/AKT/mTOR Pathway Alterations. Cancer Cell. juin 2017;31(6):820‑832.e3.

25. Vanhaesebroeck B, Guillermet-Guibert J, Graupera M, Bilanges B. The emerging mechanisms of isoform-specific PI3K signalling. Nat Rev Mol Cell Biol. mai 2010;11(5):329‑41.

bioRxiv preprint doi: https://doi.org/10.1101/777649; this version posted September 23, 2019. The copyright holder for this preprint (which was not certified by peer review) is the author/funder, who has granted bioRxiv a license to display the preprint in perpetuity. It is made available under aCC-BY-NC-ND 4.0 International license.

26. Tsujita K, Itoh T. Phosphoinositides in the regulation of actin cortex and cell migration. Biochim Biophys Acta. juin 2015;1851(6):824‑31.

27. Qian Y, Corum L, Meng Q, Blenis J, Zheng JZ, Shi X, et al. PI3K induced actin filament remodeling through Akt and p70S6K1: implication of essential role in cell migration. Am J Physiol-Cell Physiol. janv 2004;286(1):C153‑63.

28. Bai H, Li H, Li W, Gui T, Yang J, Cao D, et al. The PI3K/AKT/mTOR pathway is a potential predictor of distinct invasive and migratory capacities in human ovarian cancer cell lines. Oncotarget [Internet]. 22 sept 2015 [cité 3 févr 2018];6(28). Disponible sur: http://www.oncotarget.com/fulltext/4550

29. Campbell IG, Russell SE, Choong DYH, Montgomery KG, Ciavarella ML, Hooi CSF, et al. Mutation of the PIK3CA Gene in Ovarian and Breast Cancer. Cancer Res. 1 nov 2004;64(21):7678‑81.

30. Levine DA. Frequent Mutation of the PIK3CA Gene in Ovarian and Breast Cancers. Clin Cancer Res. 15 avr 2005;11(8):2875‑8.

31. Mayer IA, Abramson VG, Formisano L, Balko JM, Estrada MV, Sanders ME, et al. A Phase Ib Study of Alpelisib (BYL719), a PI3Kα-Specific Inhibitor, with Letrozole in ER $^{+}$/HER2 $^{-}$ Metastatic Breast Cancer. Clin Cancer Res. 1 janv 2017;23(1):26‑34.

32. André F, Ciruelos E, Rubovszky G, Campone M, Loibl S, Rugo HS, et al. Alpelisib for *PIK3CA*-Mutated, Hormone Receptor–Positive Advanced Breast Cancer. N Engl J Med. 16 mai 2019;380(20):1929‑40.

33. Jamieson S, Flanagan JU, Kolekar S, Buchanan C, Kendall JD, Lee W-J, et al. A drug targeting only p110α can block phosphoinositide 3-kinase signalling and tumour growth in certain cell types. Biochem J. 15 août 2011;438(1):53‑62.

34. Fritsch C, Huang A, Chatenay-Rivauday C, Schnell C, Reddy A, Liu M, et al. Characterization of the Novel and Specific PI3K Inhibitor NVP-BYL719 and Development of the Patient Stratification Strategy for Clinical Trials. Mol Cancer Ther. 1 mai 2014;13(5):1117‑29.

35. Jackson SP, Schoenwaelder SM, Goncalves I, Nesbitt WS, Yap CL, Wright CE, et al. PI 3-kinase p110β: a new target for antithrombotic therapy. Nat Med. mai 2005;11(5):507‑14.

36. Barlaam B, Cosulich S, Degorce S, Fitzek M, Green S, Hancox U, et al. Discovery of (R)-8-(1-(3,5-Difluorophenylamino)ethyl)-N , N -dimethyl-2-morpholino-4-oxo-4 H -chromene-6-carboxamide (AZD8186): A Potent and Selective Inhibitor of PI3Kβ and PI3Kδ for the Treatment of PTEN-Deficient Cancers. J Med Chem. 22 janv 2015;58(2):943‑62.

37. Friedrich J, Ebner R, Kunz-Schughart LA. Experimental anti-tumor therapy in 3-D: Spheroids – old hat or new challenge? Int J Radiat Biol. janv 2007;83(11‑12):849‑71.

38. Latifi A, Luwor RB, Bilandzic M, Nazaretian S, Stenvers K, Pyman J, et al. Isolation and Characterization of Tumor Cells from the Ascites of Ovarian Cancer Patients: Molecular Phenotype of Chemoresistant Ovarian Tumors. Hawkins SM, éditeur. PLoS ONE. 8 oct 2012;7(10):e46858.

bioRxiv preprint doi: https://doi.org/10.1101/777649; this version posted September 23, 2019. The copyright holder for this preprint (which was not certified by peer review) is the author/funder, who has granted bioRxiv a license to display the preprint in perpetuity. It is made available under aCC-BY-NC-ND 4.0 International license.

39. Pons-Tostivint E, Thibault B, Guillermet-Guibert J. Targeting PI3K Signaling in Combination Cancer Therapy. Trends Cancer. juin 2017;3(6):454‑69.

40. Ohie S, Udagawa Y, Kozu A, Komuro Y, Aoki D, Nozawa S, et al. Cisplatin sensitivity of ovarian cancer in the histoculture drug response assay correlates to clinical response to combination chemotherapy with cisplatin, doxorubicin and cyclophosphamide. Anticancer Res. juin 2000;20(3B):2049‑54.

41. Liao J, Qian F, Tchabo N, Mhawech-Fauceglia P, Beck A, Qian Z, et al. Ovarian Cancer Spheroid Cells with Stem Cell-Like Properties Contribute to Tumor Generation, Metastasis and Chemotherapy Resistance through Hypoxia-Resistant Metabolism. Orsulic S, éditeur. PLoS ONE. 7 janv 2014;9(1):e84941.

42. Bakrin N, Bereder JM, Decullier E, Classe JM, Msika S, Lorimier G, et al. Peritoneal carcinomatosis treated with cytoreductive surgery and Hyperthermic Intraperitoneal Chemotherapy (HIPEC) for advanced ovarian carcinoma: a French multicentre retrospective cohort study of 566 patients. Eur J Surg Oncol J Eur Soc Surg Oncol Br Assoc Surg Oncol. déc 2013;39(12):1435‑43.

43. Goéré D, Malka D, Tzanis D, Gava V, Boige V, Eveno C, et al. Is there a possibility of a cure in patients with colorectal peritoneal carcinomatosis amenable to complete cytoreductive surgery and intraperitoneal chemotherapy? Ann Surg. juin 2013;257(6):1065‑71.

44. Singh S, Armstrong A, Robke J, Waggoner S, Debernardo R. Hyperthermic Intra-Thoracic Chemotherapy (HITeC) for the management of recurrent ovarian cancer involving the pleural cavity. Gynecol Oncol Case Rep. août 2014;9:24‑5.

45. van Driel WJ, Koole SN, Sikorska K, Schagen van Leeuwen JH, Schreuder HWR, Hermans RHM, et al. Hyperthermic Intraperitoneal Chemotherapy in Ovarian Cancer. N Engl J Med. 18 janv 2018;378(3):230‑40.

46. Manzanedo I, Pereira F, Pérez-Viejo E, Serrano Á, Hernández-García M, Martínez-Torres B, et al. Hyperthermic intraoperative intraperitoneal chemotherapy (HIPEC) with primary or secondary cytoreductive surgery in the treatment of advanced epithelial ovarian cancer. Minerva Ginecol. avr 2017;69(2):119‑27.

47. McKenzie AJ, Hicks SR, Svec KV, Naughton H, Edmunds ZL, Howe AK. The mechanical microenvironment regulates ovarian cancer cell morphology, migration, and spheroid disaggregation. Sci Rep [Internet]. déc 2018 [cité 26 juin 2018];8(1). Disponible sur: http://www.nature.com/articles/s41598-018-25589-0

48. Nagelkerke A, Bussink J, Sweep FCGJ, Span PN. Generation of multicellular tumor spheroids of breast cancer cells: How to go three-dimensional. Anal Biochem. juin 2013;437(1):17‑9.

49. Nath S, Devi GR. Three-dimensional culture systems in cancer research: Focus on tumor spheroid model. Pharmacol Ther. juill 2016;163:94‑108.

50. Matte I, Legault CM, Garde-Granger P, Laplante C, Bessette P, Rancourt C, et al. Mesothelial cells interact with tumor cells for the formation of ovarian cancer multicellular spheroids in peritoneal effusions. Clin Exp Metastasis. déc 2016;33(8):839‑52.

bioRxiv preprint doi: https://doi.org/10.1101/777649; this version posted September 23, 2019. The copyright holder for this preprint (which was not certified by peer review) is the author/funder, who has granted bioRxiv a license to display the preprint in perpetuity. It is made available under aCC-BY-NC-ND 4.0 International license.

51. Campa CC, Ciraolo E, Ghigo A, Germena G, Hirsch E. Crossroads of PI3K and Rac pathways. Small GTPases. 3 avr 2015;6(2):71‑80.

52. Kim S, Kim B, Song YS. Ascites modulates cancer cell behavior, contributing to tumor heterogeneity in ovarian cancer. Cancer Sci. sept 2016;107(9):1173‑8.

53. Ayuso JM, Basheer HA, Monge R, Sánchez-Álvarez P, Doblaré M, Shnyder SD, et al. Study of the Chemotactic Response of Multicellular Spheroids in a Microfluidic Device. Rao CV, éditeur. PLOS ONE. 7 oct 2015;10(10):e0139515.

54. Shield K, Ackland ML, Ahmed N, Rice GE. Multicellular spheroids in ovarian cancer metastases: Biology and pathology. Gynecol Oncol. avr 2009;113(1):143‑8.

55. Burleson KM, Casey RC, Skubitz KM, Pambuccian SE, Oegema TR, Skubitz AP. Ovarian carcinoma ascites spheroids adhere to extracellular matrix components and mesothelial cell monolayers. Gynecol Oncol. avr 2004;93(1):170‑81.

56. Lien EC, Dibble CC, Toker A. PI3K signaling in cancer: beyond AKT. Curr Opin Cell Biol. avr 2017;45:62‑71.

57. Usui A, Ko SY, Barengo N, Naora H. P-Cadherin Promotes Ovarian Cancer Dissemination Through Tumor Cell Aggregation and Tumor–Peritoneum Interactions. Mol Cancer Res. avr 2014;12(4):504‑13.

58. Saias L, Gomes A, Cazales M, Ducommun B, Lobjois V. Cell-Cell Adhesion and Cytoskeleton Tension Oppose Each Other in Regulating Tumor Cell Aggregation. Cancer Res. 15 juin 2015;75(12):2426‑33.

59. van Baal JOAM, van Noorden CJF, Nieuwland R, Van de Vijver KK, Sturk A, van Driel WJ, et al. Development of Peritoneal Carcinomatosis in Epithelial Ovarian Cancer: A Review. J Histochem Cytochem. févr 2018;66(2):67‑83.

60. Steinkamp MP, Winner KK, Davies S, Muller C, Zhang Y, Hoffman RM, et al. Ovarian Tumor Attachment, Invasion, and Vascularization Reflect Unique Microenvironments in the Peritoneum: Insights from Xenograft and Mathematical Models. Front Oncol [Internet]. 2013 [cité 16 juin 2018];3. Disponible sur: http://journal.frontiersin.org/article/10.3389/fonc.2013.00097/abstract

61. Sant S, Johnston PA. The production of 3D tumor spheroids for cancer drug discovery. Drug Discov Today Technol. mars 2017;23:27‑36.

62. Delarue M, Montel F, Vignjevic D, Prost J, Joanny J-F, Cappello G. Compressive Stress Inhibits Proliferation in Tumor Spheroids through a Volume Limitation. Biophys J. oct 2014;107(8):1821‑8.

63. Klymenko Y, Wates RB, Weiss-Bilka H, Lombard R, Liu Y, Campbell L, et al. Modeling the effect of ascites-induced compression on ovarian cancer multicellular aggregates. Dis Model Mech. 1 sept 2018;11(9):dmm034199.

bioRxiv preprint doi: https://doi.org/10.1101/777649; this version posted September 23, 2019. The copyright holder for this preprint (which was not certified by peer review) is the author/funder, who has granted bioRxiv a license to display the preprint in perpetuity. It is made available under aCC-BY-NC-ND 4.0 International license.

64. Raghavan S, Ward MR, Rowley KR, Wold RM, Takayama S, Buckanovich RJ, et al. Formation of stable small cell number three-dimensional ovarian cancer spheroids using hanging drop arrays for preclinical drug sensitivity assays. Gynecol Oncol. juill 2015;138(1):181‑9.

Figure legends:

Figure 1: Modeling tumour aggregates derived from ovarian cancer ascites. (A) High grade ovarian serous carcinoma immunohistochemistry taken from ovary and ascites fluid, in which tumourospheres are indicated by arrows, (x100 and x400 magnification). PAP = Papanicolaou, MGG = May-Grünwald-Giemsa, PAS = Periodic Acid Schieff. (B) Survival curves from patients with high grade serous ovarian cancer presenting a rich or poor aggregate number in ascites; 12 patients. (C) Patient tumourosphere morphology evolution 1, 4 or 7 days after seeding. (D) Model of transcoelomic dissemination from the primary tumour facilitated by the flow of liquid and formation of tumourospheres. (E) Morphology and (F) area of SKOV-3 GFP tumorospheres. Measurements with ZEN® software (5X magnification, fluorescence, $n \geq 2$). Comparison of 5000 and 10000 SKOV-3 GFP tumorosphere area on day 14 by Student t-test $p < 0.01$ (**). (G) Evolution of (left) living cells number by Alamar Blue assay and (right) GFP fluorescence over time in 5000 SKOV-3 GFP cells tumorospheres, (H) Morphology of heterotypic tumourospheres composed by 5000 SKOV-3 GFP cells (green) cultured with or without different numbers of MSC (5, 50, 500, 5000) 1, 4 or 7 days after seeding.

Figure 2: PI3Kα inhibition prevents ovarian cancer cell tumourosphere formation. (A) 5,000 SKOV-3 GFP cells which will form tumouropheres at d1 are treated or not at d0 and d4 with A66 and BYL719 (1 and 10 µM) or cisplatin (0.5 and 5 µM). (B) SKOV-3 cells are serum-deprived overnight, pre-treated for 1 hour with specific PI3Kα inhibitors and then serum-activated for 15 minutes. Actin-standardized quantification of (C) phospho-Akt (S473) and (D) phospho-Akt (T308) amount relative to the control condition (without treatment). (E, F) SKOV-3 GFP tumourospheres are treated according to the (A) schedule and morphology is observed 1, 4 or 7 days after seeding. (G, H) Area or (I, J) fluorescence intensity are evaluated at d1, d4 and d7 using Zen® software (5X magnification), $n \geq 3$, Mean +/- SEM (ANOVA test compared to corresponding observation day control condition, $p < 0.001$ (***), $p < 0.01$ (**), $p < 0.05$ (*)).

Figure 3: PI3Kα selective inhibition prevents ovarian cancer cell tumourosphere maintenance. (A) 5,000 SKOV-3 GFP cells tumourospheres are treated or not at d1 and d4 with A66, BYL719, TGX-221 or AZD8186 (0.01, 0.1, 1 and 10 µM) or cisplatin (0.5 and 5 µM). (B and G) Tumourospheres morphology is evaluated on d1, d4 and d7. (C-F and H) Tumourosphere area is evaluated on d1, d4 and d7 using Zen® software (5X magnification), $n \geq 3$, Mean +/- SEM (ANOVA test compared to the corresponding observation day control condition, $p < 0.001$ (***), $p < 0.01$ (**), $p < 0.05$ (*)).

Figure 4: Only PI3Kα inhibition impacts ovarian tumour cell viability in 3D culture. (A) 5,000 SKOV-3 GFP cells tumourospheres are treated or not at d1 and d4 with A66, BYL719, TGX-221 or AZD8186 (0.01, 0.1, 1 and 10 µM) or cisplatin (0.5 and 5 µM). Living cells percentage is evaluated on d7 by (B, C) MTT test and by (D, E) Alamar Blue® test (3D), $n \geq 3$. (F) Tumourosphere morphology is evaluated on d7 using Zen® software (in fluorescence, 5X magnification), living cells are marked with Calcein (white), $n \geq 3$. (G and H) Living cells occupied area after treatment is quantified using the ImageJ® software $n = 2$. Mean +/- SEM (ANOVA test compared to the corresponding observation day control condition, $p < 0.001$ (***), $p < 0.01$ (**), $p < 0.05$ (*)).

Figure 5: PI3K inhibitors sensitize 3D cultured cells to low concentration cisplatin antitumoural effect. 5,000 SKOV-3 cells tumoursospheres are treated or not on d1 and d4 after seeding with a fixed concentration of 1 µM of A66, BYL719, TGX-221, or AZD8186 combined or not with increased

bioRxiv preprint doi: https://doi.org/10.1101/777649; this version posted September 23, 2019. The copyright holder for this preprint (which was not certified by peer review) is the author/funder, who has granted bioRxiv a license to display the preprint in perpetuity. It is made available under aCC-BY-NC-ND 4.0 International license.

concentrations of cisplatin (0.05, 0.5, 5µM). (A) Tumourosphere morphology and (C) area ($n \geq 3$) are evaluated using Zen® software (in fluorescence, 5X magnification). (D) Living cells percentage is evaluated on day 7 by Alamar Blue® test ($n \geq 3$). (B) living cells are marked with Calcein and (E) Living cells occupied area after treatment is quantified using ImageJ® software (n = 2), Mean +/- SEM (ANOVA test compared to cisplatin concentration and corresponding observation day condition, $p < 0.001$ (***), $p < 0.01$ (**), $p < 0.05$ (*)).

Figure 6: PI3Kα inhibitors remain efficient in tumourospheres compacted by mesenchymal stem cells. 5,000 SKOV-3 GFP cells (green) associated with different MSC ratios (labeled in red using Quantum Dots) tumourospheres are performed and treated with 1 or 10 µM of A66 or BYL719. (A) Tumourospheres morphology and (B) area (n = 3) are evaluated using Zen® software (in fluorescence, 5X magnification) on d7. Mean +/- SEM

Figure 7: Schematic representation of PI3Kα involvement in tumour cell aggregates from ascites. 1) Known involvement of PI3Kα on ovarian primary tumor. 2) PI3Kα participates in tumourosphere formation within the peritoneum (treatment with PI3Kα inhibitors causing a delay in the clusters formation). 3) PI3Kα participates in the maintenance of tumourospheres and in resistance to conventional treatment of peritoneal carcinomatosis. PI3Kα is a target to prevent transcoelomic dissemination and maintenance of tumour cells for ovarian cancer patients.

Supplementary Figure 1: Development of heterotypic tumourospheres. (A) Area and (B) morphology of MSC tumourospheres. Measurements with ZEN® software (5X magnification, $n \geq 2$). (C) Observation of fibrous-like structure formations within MSC aggregates. 5000 SKOV-3 cells GFP cells associated with different MSC ratios (5, 50, 500 or 5000) were seeded and (D) area and (E) GFP fluorescence intensity are evaluated at d1, d4 and d7 using Zen® software (in fluorescence, 5X magnification, n = 3). (F) observation of heterotypic tumourospheres of SKOV-3 cells (green) and MSC (red). Mean +/- SEM (ANOVA test in comparison with the condition without MSC at corresponding observation day, $p < 0.001$ (***), $p < 0.01$ (**), $p < 0.05$ (*)).

Supplementary Figure 2: Effects of PI3K inhibitors and cisplatin on SKOV-3 tumourospheres. 5000 SKOV-3 cells tumourospheres are produced and treated or not with A66, BYL719, TGX-221, AZD8186 or cisplatin 24h after seeding. (A, B) Living cells percentage is evaluated on d4 by Alamar Blue® test. (C) Living cells are marked with Calcein (green) and dead cells with EthD-1 (red) thanks to the LIVE / DEAD® kit. Mean +/- SEM (n = 3).

Supplementary Figure 3: MSC tumourospheres treated with PI3K inhibitors or cisplatin. 5000 MSC tumourospheres are produced and treated or not with A66, BYL719, or cisplatin 24h after seeding. (A, B) Morphology and (C, D) area of MSC tumourospheres are measured with ZEN® software (5X magnification, n = 3).

Supplementary Table 1: Patients data. Data corresponding to the ascites samples isolated from patients. Patient number, Age (in years), histology, aggregates number (per microscopy field) and white blood cells number (per mm^3) are represented. The ascites dilution used to determine the aggregates number is adjusted with the white blood cells number (for further explanation, see M&M). A normalized aggregates number has been determined by multiplying these two parameters. Rich aggregates ascites have a normalized aggregates number above 100,000 while poor aggregates ascites have a normalized aggregates number below 100,000.

bioRxiv preprint doi: https://doi.org/10.1101/777649; this version posted September 23, 2019. The copyright holder for this preprint (which was not certified by peer review) is the author/funder, who has granted bioRxiv a license to display the preprint in perpetuity. It is made available under aCC-BY-NC-ND 4.0 International license.

Figures:

bioRxiv preprint doi: https://doi.org/10.1101/777649; this version posted September 23, 2019. The copyright holder for this preprint (which was not certified by peer review) is the author/funder, who has granted bioRxiv a license to display the preprint in perpetuity. It is made available under aCC-BY-NC-ND 4.0 International license.

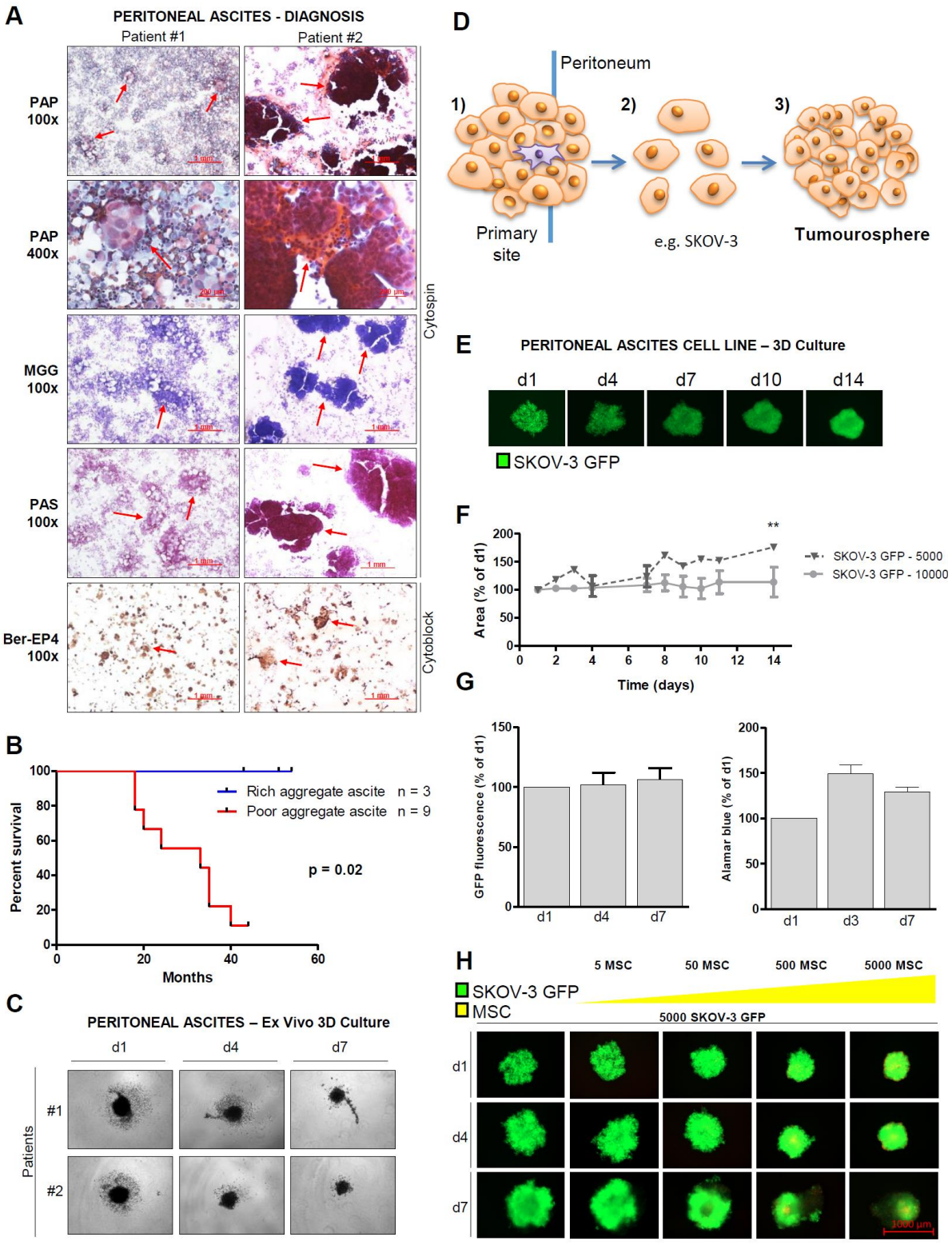

Figure 1

bioRxiv preprint doi: https://doi.org/10.1101/777649; this version posted September 23, 2019. The copyright holder for this preprint (which was not certified by peer review) is the author/funder, who has granted bioRxiv a license to display the preprint in perpetuity. It is made available under aCC-BY-NC-ND 4.0 International license.

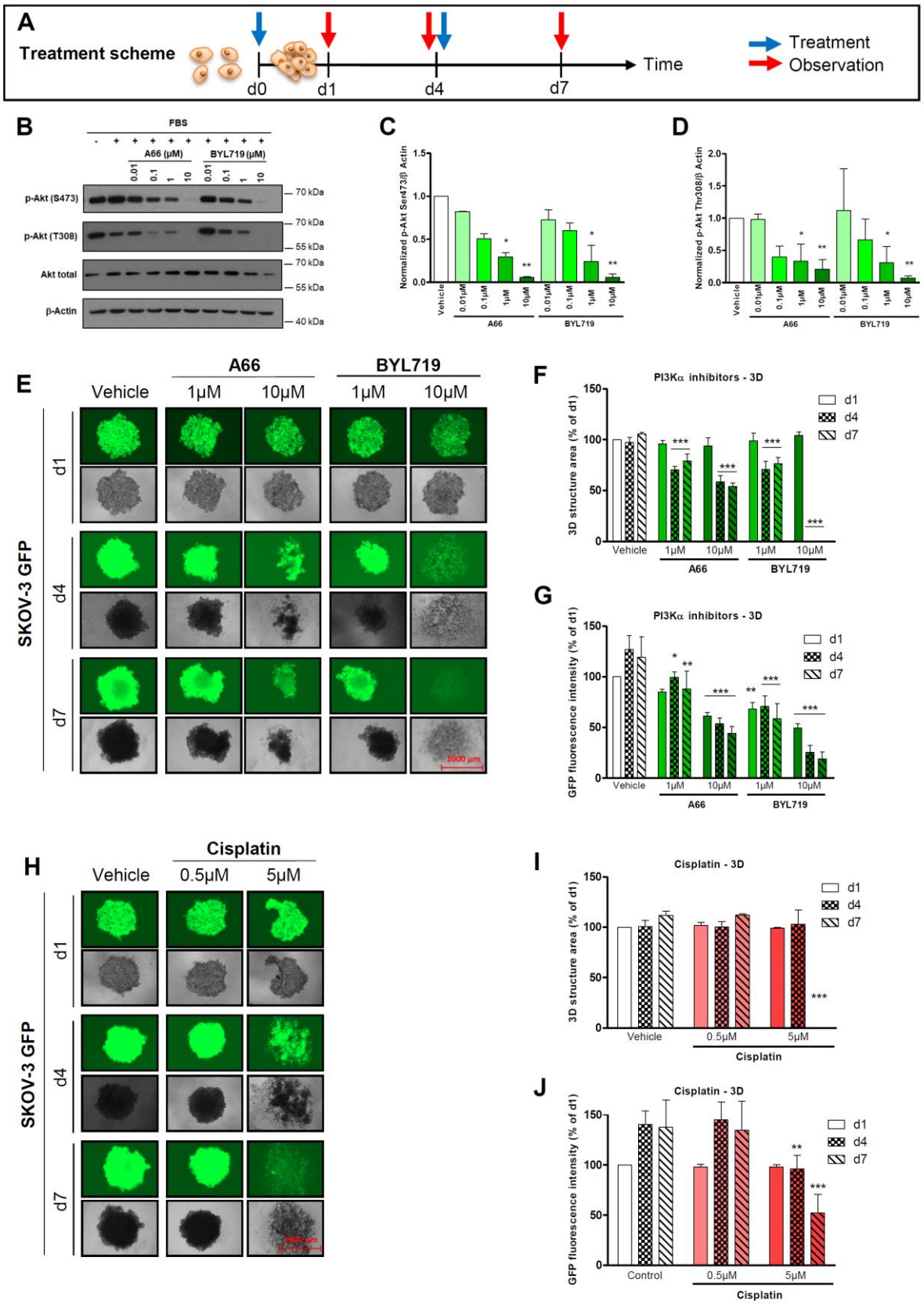

Figure 2

bioRxiv preprint doi: https://doi.org/10.1101/777649; this version posted September 23, 2019. The copyright holder for this preprint (which was not certified by peer review) is the author/funder, who has granted bioRxiv a license to display the preprint in perpetuity. It is made available under aCC-BY-NC-ND 4.0 International license.

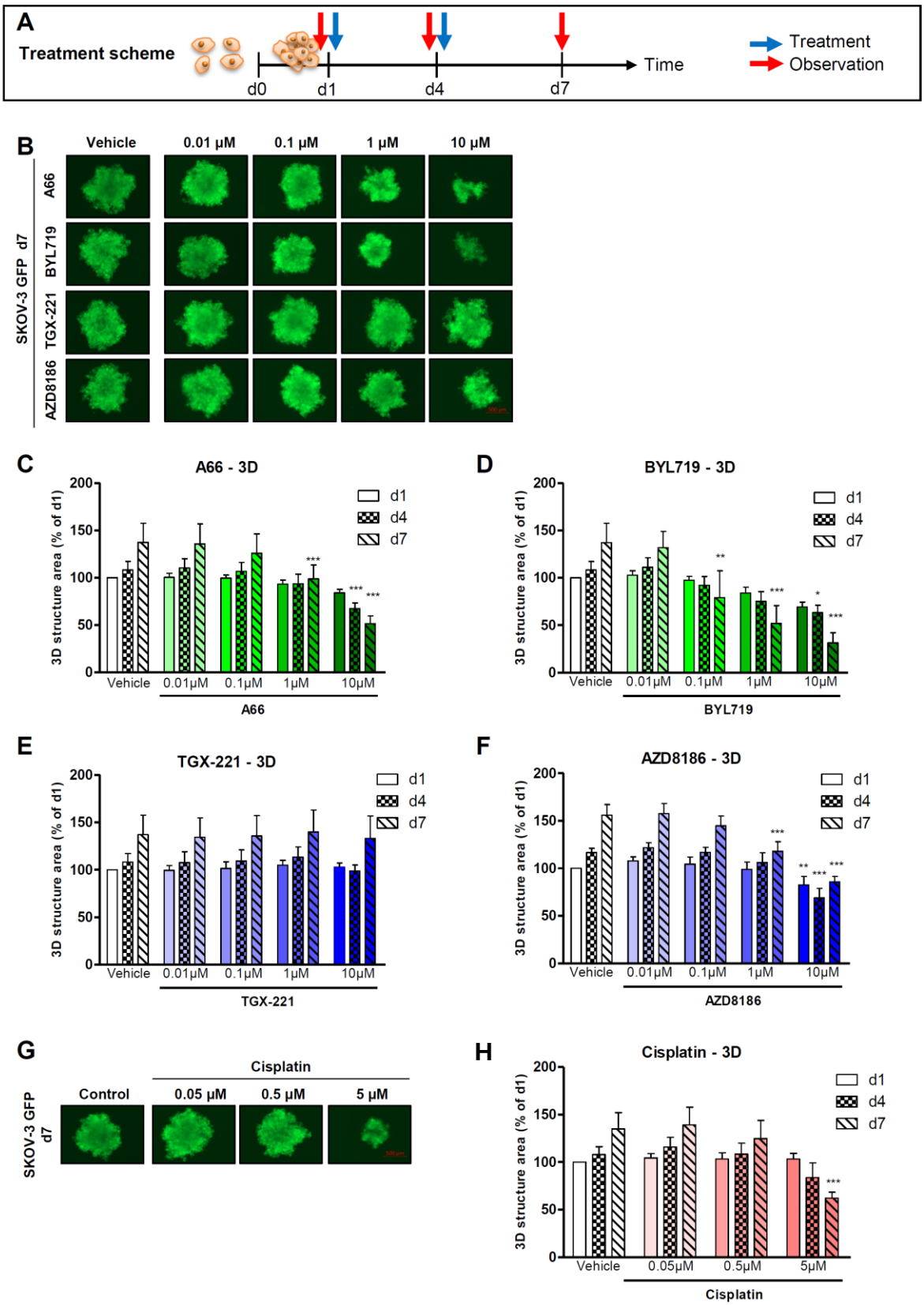

Figure 3

bioRxiv preprint doi: https://doi.org/10.1101/777649; this version posted September 23, 2019. The copyright holder for this preprint (which was not certified by peer review) is the author/funder, who has granted bioRxiv a license to display the preprint in perpetuity. It is made available under aCC-BY-NC-ND 4.0 International license.

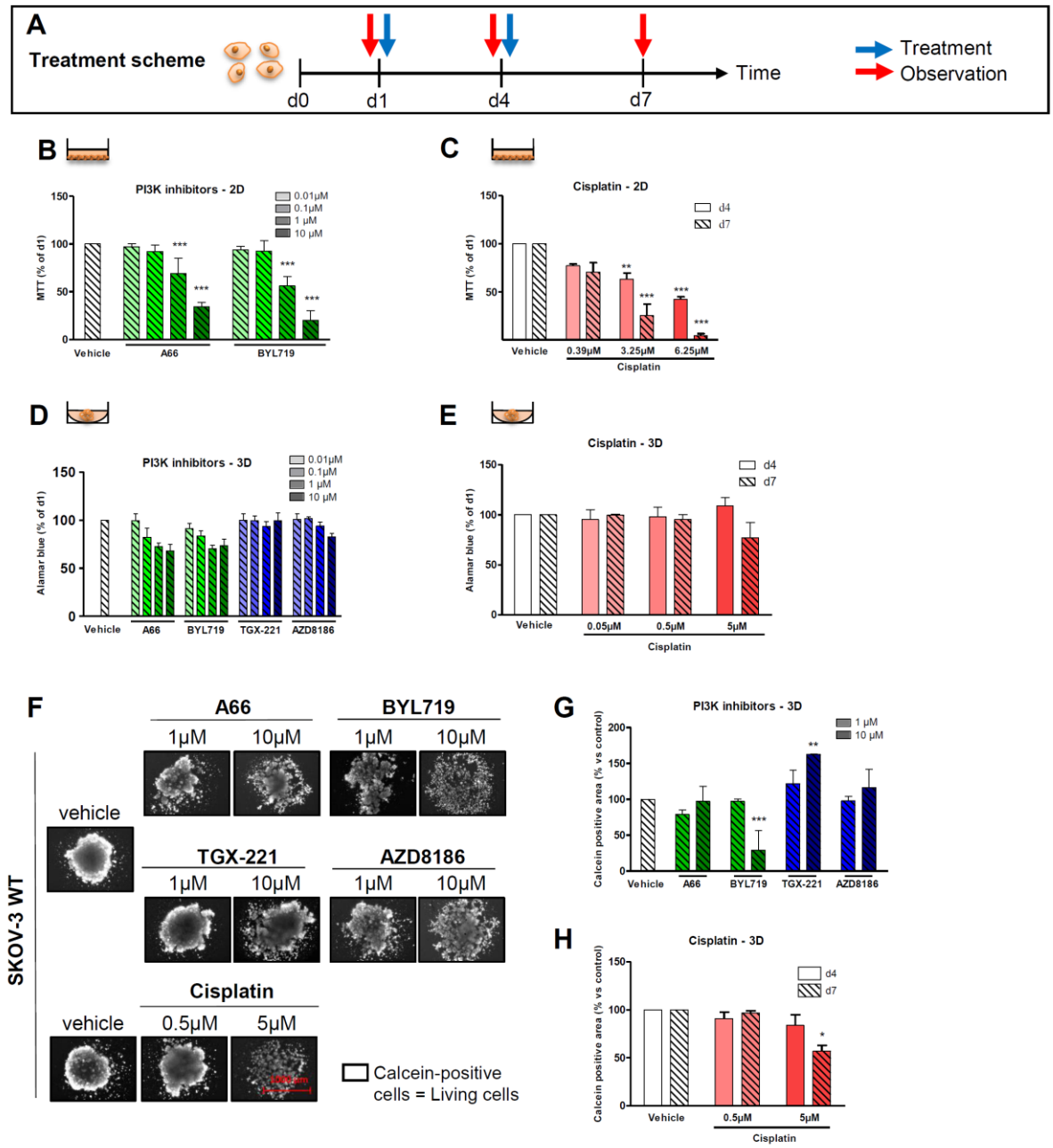

Figure 4

bioRxiv preprint doi: https://doi.org/10.1101/777649; this version posted September 23, 2019. The copyright holder for this preprint (which was not certified by peer review) is the author/funder, who has granted bioRxiv a license to display the preprint in perpetuity. It is made available under aCC-BY-NC-ND 4.0 International license.

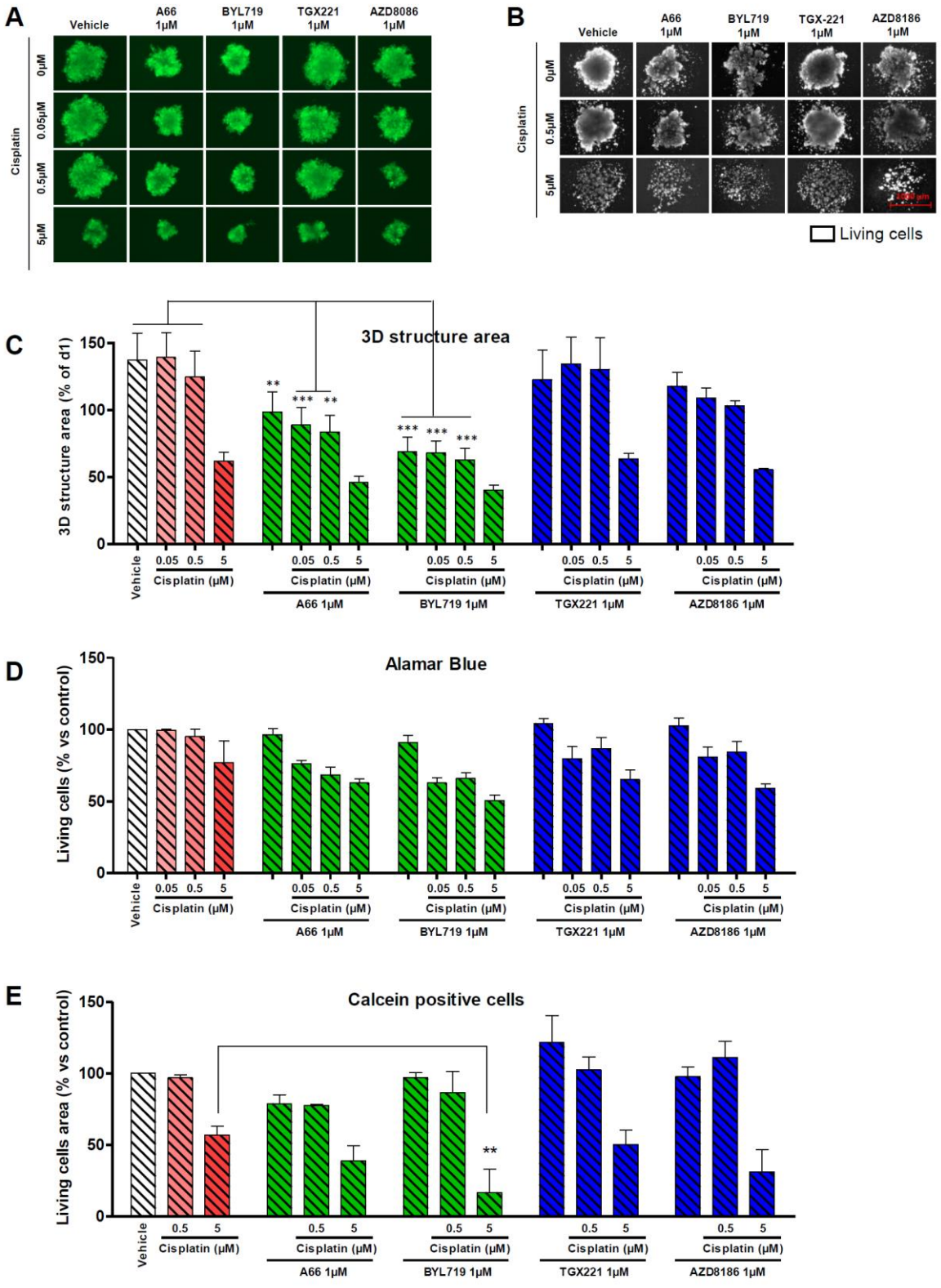

Figure 5

bioRxiv preprint doi: https://doi.org/10.1101/777649; this version posted September 23, 2019. The copyright holder for this preprint (which was not certified by peer review) is the author/funder, who has granted bioRxiv a license to display the preprint in perpetuity. It is made available under aCC-BY-NC-ND 4.0 International license.

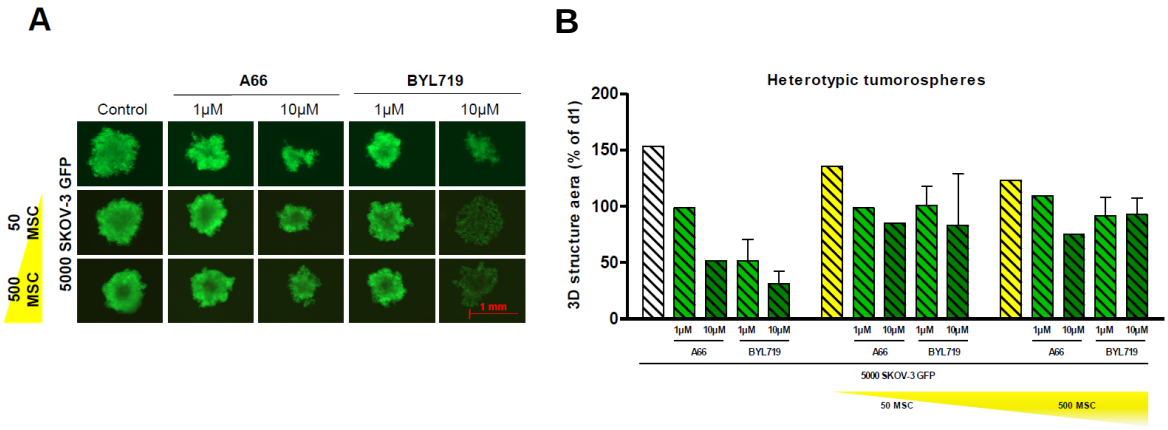

Figure 6

bioRxiv preprint doi: https://doi.org/10.1101/777649; this version posted September 23, 2019. The copyright holder for this preprint (which was not certified by peer review) is the author/funder, who has granted bioRxiv a license to display the preprint in perpetuity. It is made available under aCC-BY-NC-ND 4.0 International license.

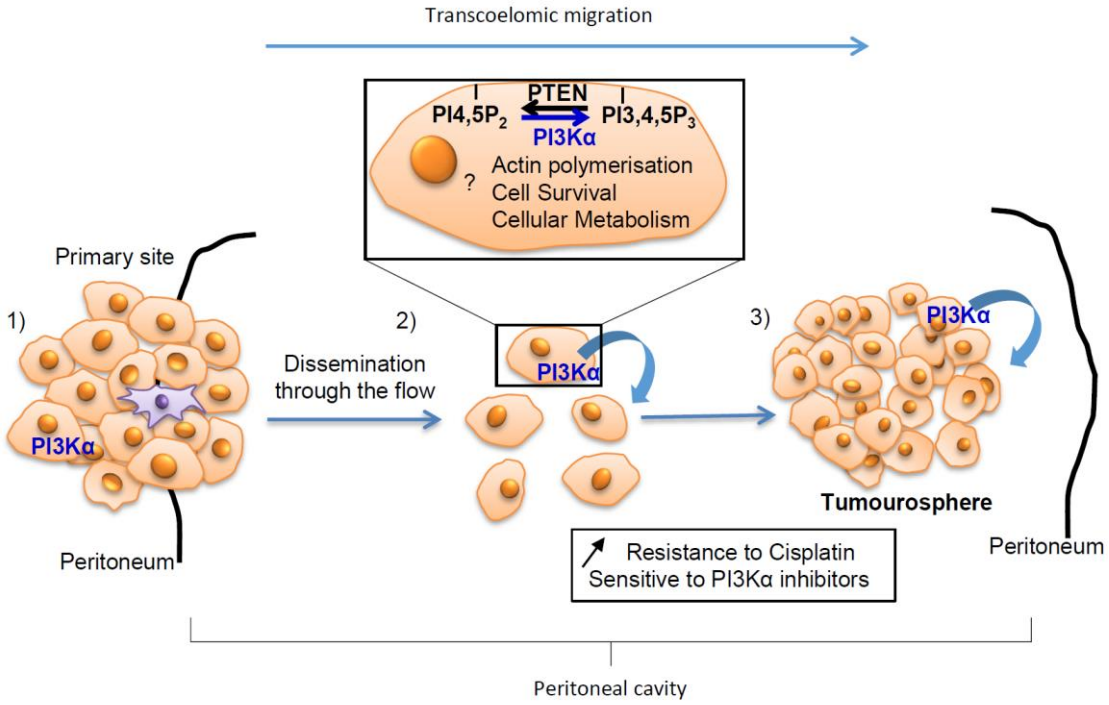

Figure 7

bioRxiv preprint doi: https://doi.org/10.1101/777649; this version posted September 23, 2019. The copyright holder for this preprint (which was not certified by peer review) is the author/funder, who has granted bioRxiv a license to display the preprint in perpetuity. It is made available under aCC-BY-NC-ND 4.0 International license.

Supporting information:

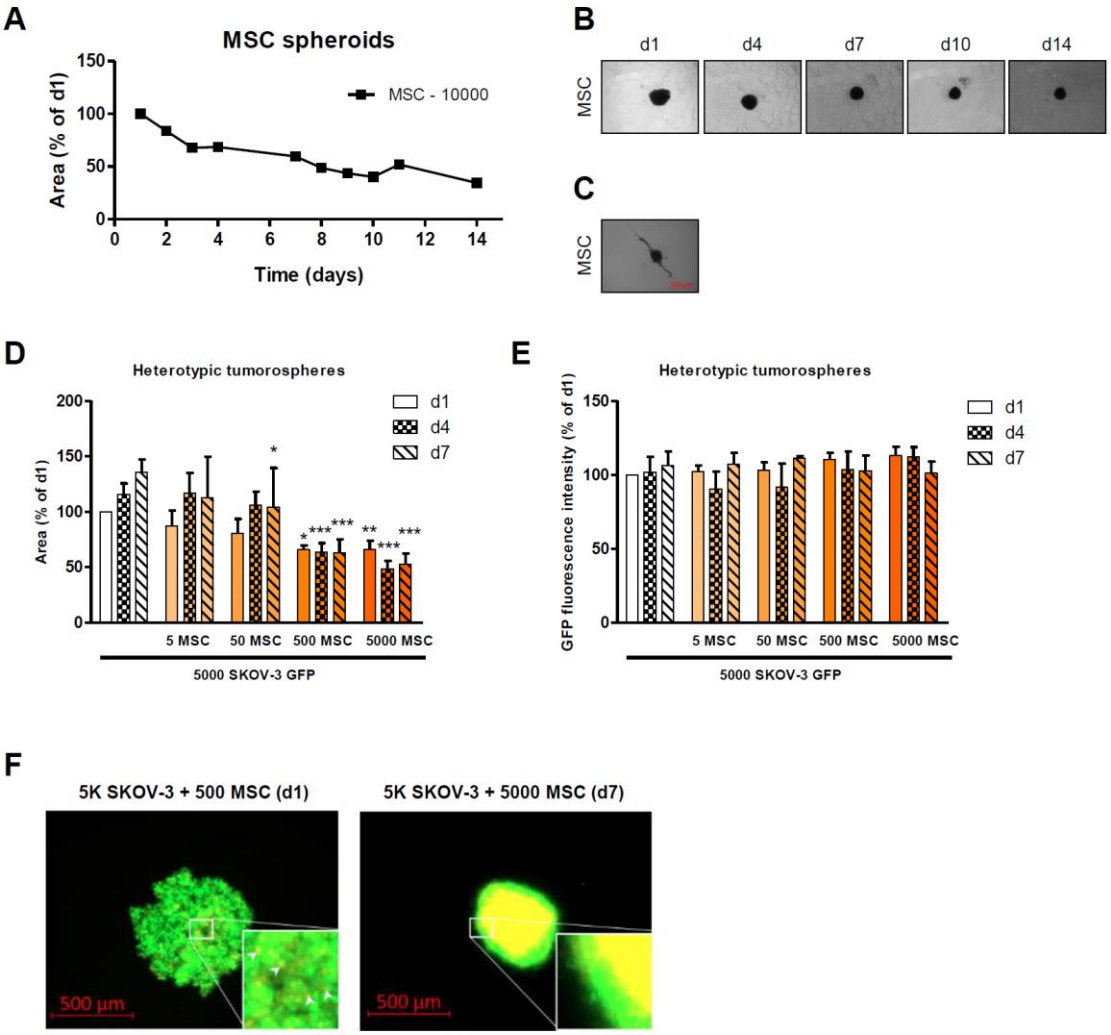

Supplementary Figure 1

bioRxiv preprint doi: https://doi.org/10.1101/777649; this version posted September 23, 2019. The copyright holder for this preprint (which was not certified by peer review) is the author/funder, who has granted bioRxiv a license to display the preprint in perpetuity. It is made available under aCC-BY-NC-ND 4.0 International license.

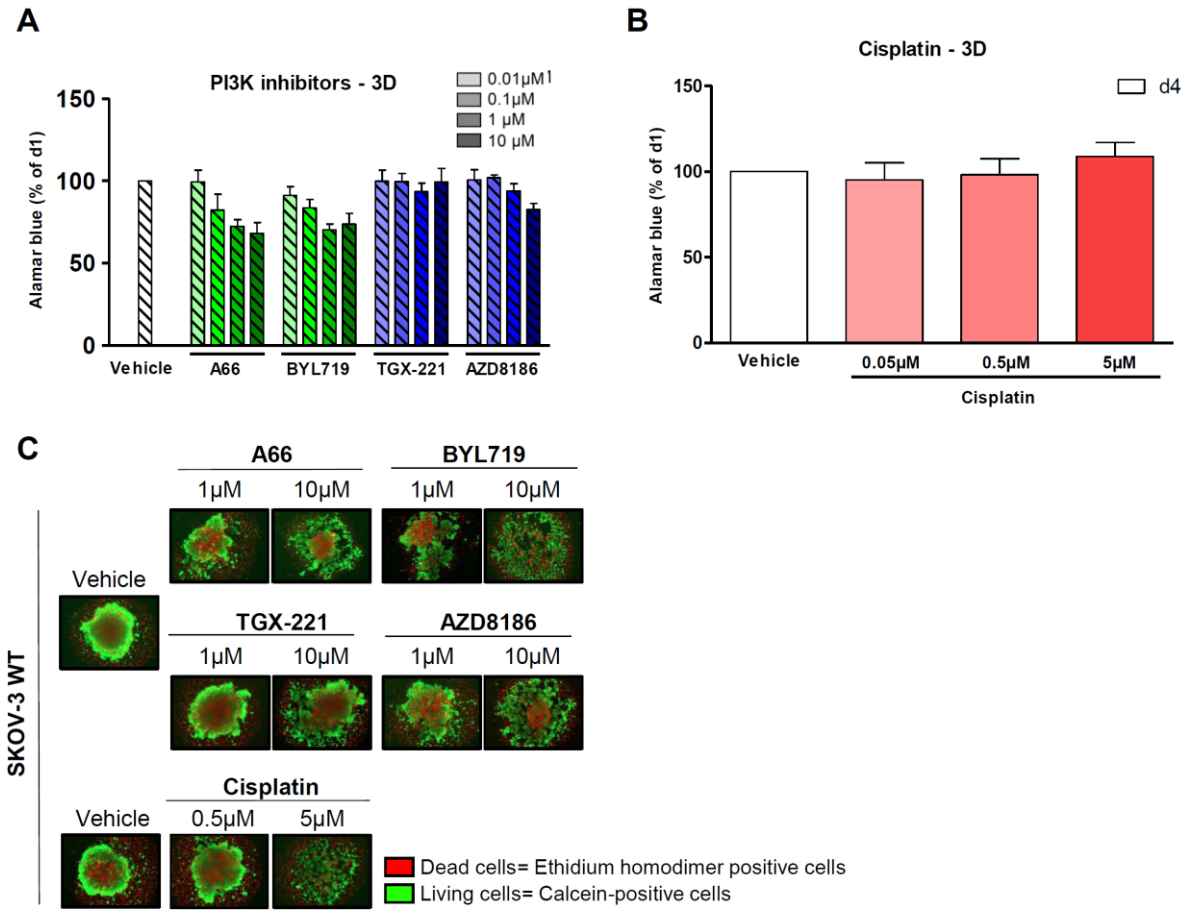

Supplementary Figure 2

bioRxiv preprint doi: https://doi.org/10.1101/777649; this version posted September 23, 2019. The copyright holder for this preprint (which was not certified by peer review) is the author/funder, who has granted bioRxiv a license to display the preprint in perpetuity. It is made available under aCC-BY-NC-ND 4.0 International license.

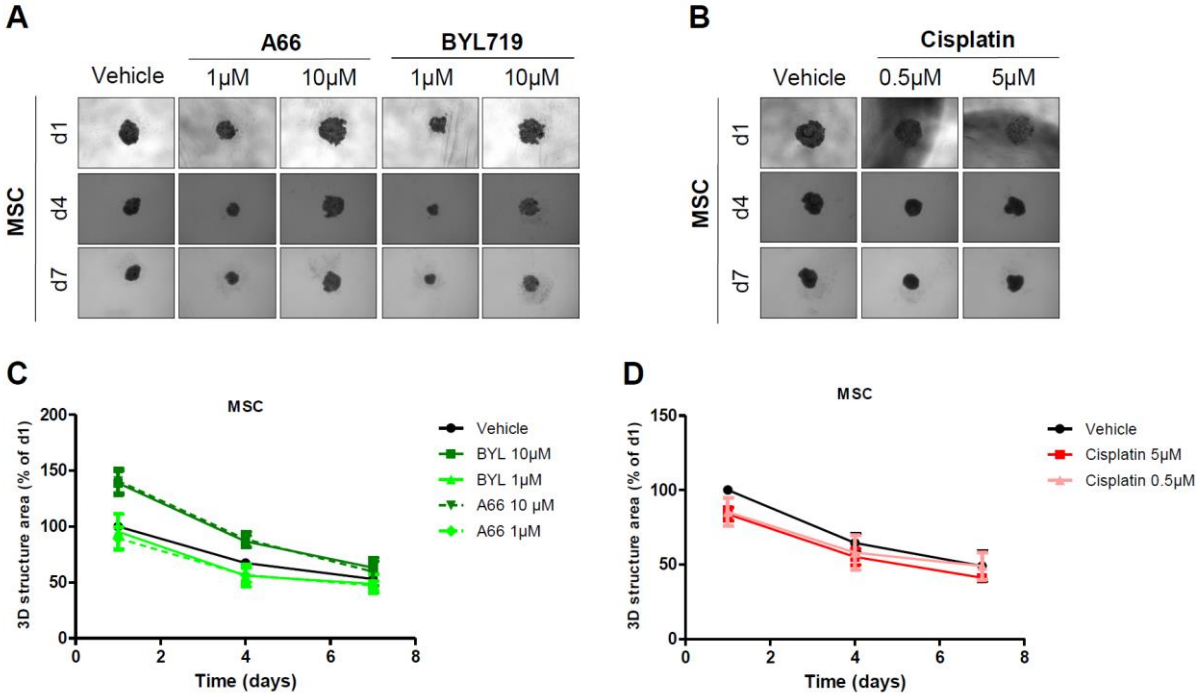

Supplementary Figure 3

bioRxiv preprint doi: https://doi.org/10.1101/777649; this version posted September 23, 2019. The copyright holder for this preprint (which was not certified by peer review) is the author/funder, who has granted bioRxiv a license to display the preprint in perpetuity. It is made available under aCC-BY-NC-ND 4.0 International license.

Patient #	Age (years)	Histology	Aggregates number (per field)	White blood cells number (per mm^3)	Normalized aggregates number	Aggregates density
1	72	high grade serous	12	350	4200	Poor
2	65	high grade serous	12	1000	12000	Poor
3	70	high grade serous	3	1350	4050	Poor
4	61	high grade serous	120	4000	480000	Rich
5	57	high grade serous	104	1300	135200	Rich
6	66	high grade serous	23	2500	57500	Poor
7	65	high grade serous	3	1200	3600	Poor
8	73	high grade serous	36	7500	270000	Rich
9	58	high grade serous	5	2500	12500	Poor
10	61	high grade serous	3	6500	19500	Poor
11	62	high grade serous	12	2950	35400	Poor
12	56	high grade serous	8	510	4080	Poor

Supplementary Table 1